USAFA-TN-82-4

Department of Aeronautics
Dean of the Faculty
United States Air Force Academy
Colorado 80840

MEASUREMENT OF WAKE INTERACTIONS OF A CANARD AND A FORWARD SWEPT WING

TECHNICAL NOTE
USAFA-TN-82-4

Griffin, K.E.

6 JULY 1982

APPROVED FOR PUBLIC RELEASE: DISTRIBUTION UNLIMITED

82   071

Any views expressed in this paper are those of the author. They should not be interpreted as reflecting the views of the USAF Academy or the official opinion of any governmental agency. Notes are not reviewed for content or quality by the USAF Academy but are published primarily as a service to the faculty to facilitate internal research communication.

This Technical Note has been cleared for open publication and/or public release by the appropriate Office of Information in accordance with AFR 190-17 and DODD 5230.9. There is no objection to unlimited distribution of this Technical Note to the public at large or by DDC to the National Technical Information Service.

This Technical Note is approved for publication.

Clayton V. Stewart, Lt Colonel, USAF
Director of Research and Continuing Education

1

FORWARD

This technical note is a report on the forward-swept wing
research conducted by the Aeronautical Laboratory at the United
States Air Force Academy during the period from 22 July 81 to 30
September 81. This technical effort was sponsored by the Defense
Advanced Projects Agency (DARPA) and administered as ARPA 4364 by
Col James Allburn. Capt K.E. Griffin, the principal investigator,
was assisted by the staff and cadets at the Air Force Academy.

The summary report is accompanied by plots of the various flow
fields around and in the wake of a forward-swept wing aircraft
configuration both with and without a leading canard. Specific
pressure and velocity data for various wind tunnel locations and
model configurations are contained in the Appendix. The summary
report should be used as a guide to locate and interpret the
specific data documented in the Appendix.

2

MEASUREMENT OF WAKE INTERACTIONS OF A CANARD AND A FORWARD-SWEPT WING

K.E. Griffin*

Abstract

This report presents experimental lifting surface wake data taken from a canard/forward-swept wing reflecting plane wind tunnel model. The data includes distributions of total, dynamic, and static pressures as well as cross velocity magnitudes and directions for an array of points around the model, both near the model and in its freestream wake. The model was tested as a body alone, as a wing/body combination, and as a wing/body/canard combination in order to compare wing wakes to wing/canard wakes.

I. Introduction

Current design results indicate that a canard used as the trimming surface for the highly maneuverable fighter category applications of the forward-swept wing concept has advantages over a conventional aft-mounted horizontal tail. These advantages are due in part to improvements in the lift capability of the wing and the location of the canard lift vector relative to the wing lift vector. Since some of these advantages rely on the interaction of the canard wake with the wing flow field, a detailed understanding of the lifting surface wake produced by a canard and the interaction of this wake with the wing flow field is necessary. This study is the first of a series of wind tunnel tests aimed at developing a more complete understanding of these wakes and wake interactions using pressure and velocity data taken in the free airstream around canard-configured forward-swept wing configurations.

*Captain, USAF, Assistant Professor of Aeronautics, DFAN

The effects of a canard wake on an aft-mounted primary
lifting surface had not been thoroughly examined until recently
because conventional tail placement did not require detailed
knowledge of these effects. For conventional horizontal tail
placement, the primary lifting surface is not in the wake of any
other lifting surface. The horizontal tail is not used to provide
part of the lift but only for stability and control. Furthermore,
for conventional tail locations, the wing tip disturbances in the
wing wake are outboard of the horizontal tail. The horizontal
tail primarily sees a rather uniform downwash from the wing,
which can be compensated for with adjustments to the horizontal
tail angle-of-attack.

The canard configuration for a trimming device and its
associated wake has more significant effects. Its tip
disturbances and wake pass directly through the near flow field
of the wing, with the aircraft angle-of-attack attitude dictating
how close these disturbances will actually come to the wing.
These disturbances can have an effect on the lift distribution,
separation characteristics, and drag production of the wing.
Depending on the relative amount of lift to be produced by the
canard for any given g condition and the geometric locations of
wing and canard, the canard effects on the wing can vary in
intensity. When the additional canard lift perturbations for
stability and control are added to its wake from steady state
lift, the wing near flow field may even vary with pilot or
stability inputs for simple cruise flight.

4

In order to shed light on these interactions this report contains flow field data describing wake characteristics of the canard and forward-swept wing configuration shown in Figure 1. The data includes total, static, and dynamic pressures plus cross velocity magnitudes and directions for arrays of data points organized in planes whose unit normals are parallel to the freestream direction. This data was collected using the seven-hole pressure probe and associated computer software developed at the United States Air Force Academy and described in detail in Ref. 1.

Using the total pressure plots to document the wake and vortex locations and the cross veiocity data to determine the wake downwash and the sense of vortex rotation, comparisons of wing flow fields with and without the canard can illustrate how ...e canard wakes i. reract with the wing flow field. These comparisons in qualitative form are possible with the graphical data included in this document. Detailed pressure and velocity numbers for points in the flow are available in the Appendix.

In this report the position of a lifting surface wake is determined by the loss of energy in the region of the wake. In the wake the loss of total pressure is representative of this energy loss and occurs due to viscosity effects upstream on the wing surface. Viscosity becomes important in the large velocity gradients that are developed in the boundary layers on the wing. Gradients in velocity are formed when the air particles passing over the upper and lower surfaces of a lifting wing form the

5

boundary layer transition from free flow to zero relative velocity at that surface. Because this total pressure drop exists in the wing wake, the wake location can be documented by noting this signature in the loss in total pressure aft of lifting surfaces. This total pressure drop can be subtle, especially at low angles of attack; therefore, good resolution of flow field pressures is required to detect the wake.

In a similar fashion to the wing wake, strong concentrations of vorticity in a flow field can dissipate energy. In the region near the core or centerline of highly rotational flow, the crossflow velocity gradients become very large. Crossflow as used in this study refers to the velocity component that is perpendicular to the freestream velocity vector. In regions near a vortex the crossflow vectors describe the circular or rotational component of the total flow velocity. Very close to the core of the vortex, the large velocity gradients dissipate energy through the effects of viscosity. As in the wake, this energy loss can be documented by means of the loss of total pressure in the local flow field.

These losses in total pressure are useful in locating wake characteristics only in instances where the total pressure can be measured. Traditionally these measurements have been difficult because of the large changes in flow angularity that occur in the very regions of greatest interest. Methods that employ conventional pressure probes, which directly measure static and dynamic pressure, require knowledge of the flow direction in

6

order to correctly orient the probe. Flow direction, however, is one of the unknowns which must be recovered from the wake flow field for the configuration in this study. The use of a general array of pressure ports around the conical head of a pressure probe has removed this flow angle sensitivity. Figure 2 shows a probe containing an array of 6 pressure ports located on the conical surface around a center line pressure port. The array of pressure ports provides the variety of port orientation necessary to allow pressure measurements in attached flow to be made. This can be done in flow whose freestream velocity vector describes up to an 80 degree angle with the probe centerline. Selection of the proper combination of port pressures provides both pressure and crossflow velocity information. These measurements are made possible by a set of fourth order polynomial equations that are formulated to accept the raw pressure port data and generate total, dynamic, and static pressure coefficients. Also available from these equations are crossflow velocity magnitudes and directions. These equations contain constant coefficients which are established for a particular probe in a series of calibration tests using known flow conditions and probe orientations. Ref. 1 describes this procedure in detail for the probe used in this study. This probe is approximately 0.1 inch in diameter, so that its presence does not provide a significant disturbance in the flow it is measuring for the scales of phenomena being measured.

Using the seven-hole probe, pressure and velocity measurements are taken throughout the flow field of the model of

7

interest. This requires movement of the probe to many data points in a precise manner. In order to do this in a fast and accurate way, a three degree-of-freedom traversing mechanism, shown in Figure 3, was employed. The probe was positioned using a holder riding on a series of jackscrews oriented in the three orthogonal directions of x (positive moving away from the wing plane), y (positive moving spanwise from the tip into the fuselage), and z (positive moving in the negative streamwise direction). This coordinate system is shown in Figure 4 with the system origin located at a point 3 inches directly above the wing trailing edge tip. A computer dedicated to testing hardware control (called the controller), is shown in Figure 5. The controller actuated the jackscrews through small motors and feedback potentiometers to position the probe at pre-selected locations in the flow field. This method provides accuracy and speed in surveying the large number of points used in these wake studies.

With the large number of points surveyed and the automated positioning of the probe employed, a sophisticated data management scheme was developed to make use of the speed and accuracy of the positioning system. The system used at USAFA involves another mini-computer, shown in Figure 6, to reduce the data in real time and to store all the information at each data point on a mass storage disk drive. The data-acquisition computer has the simultaneous equations of calibration coefficients mentioned earlier in a form ready to accept the seven-hole probe pressure measurements and convert them to final form pressure and

8

velocity data. The procedure is organized so that the controller moves the probe to a pre-selected location. The data computer allows the pressures to settle to steady-state conditions and then accepts the pressures from the probe. It then generates the final pressure and velocity data, stores these plus the coordinate information on disk, and signals the hardware computer to move to the next flow field location.

The data is collected in 100-point segments. After each segment is collected, graphical displays of pressure and cross velocity are possible. This allows the investigator to determine if the correct data has been taken and if the point locations were correct for the disturbance being investigated. This real time data reduction allows refinements in the flow field surveys as data is being taken without the normal delays for separate data reduction and possible retesting. Temporary data storage is made on magnetic disk for detailed data interpretation.

II. Test Configuration

A. Subsonic Wind Tunnel

These tests were performed in the 2 feet x 3 feet Subsonic Wind Tunnel at the United States Air Force Academy. This continuous flow tunnel's test section has a cross section approximately 2 feet x three feet with a length of 70 inches. The wind tunnel operating range is 0.04 - Mach number - 0.35. Local atmospheric conditions prescribe wind tunnel total temperature and pressure values, since artificial control of these inside the

9

tunnel is not available. These ambient conditions generally
provide air speeds from 50 fps to 400 fps. The above capabilities
provide Reynolds numbers in the range of .2 x 10 to 1.6 x 10 per
foot and dynamic pressures in the range of 1.89 psf (pounds per
square foot) to 130 psf.

Flow quality in the Subsonic Wind Tunnel is maintained by a
series of screens, turning vanes, and honeycomb grids. The wind
tunnel flow characteristics are documented in Ref. 4 and
summarized below:

   a. Nominal turbulence level of the test section is 0.12
      percent, based upon an overall spatial average over the
      entire speed range investigated.

   b. The freestream speed was observed to be uniform to within
      0.8 percent of an average over the entire extent of the
      test section cross section. (This represents a worst
      case value for nominal velocities investigated).

   c. Measurements of the crossflow components revealed a
      small value of the horizontal component as the side walls
      were approached (this corresponds to the physical side
      wall divergence). No vertical crossflow was observed.

B. Wind Tunnel Model

   The model used in these tests (shown in Figure 1) is a
simplified generic rigid representation of a forward-swept wing
vehicle. It was mounted in the wind tunnel ceiling as shown in
Figure 7. It is a half span or reflection plane model with the

10

general dimensions shown in Figure 4. The airfoils for both the wing and canard are bi-convex sharp leading edge airfoils with t/c ratios of 0.05 for the wing and 0.04 for the canard. Neither the wing nor the canard has any twist built into it. The model provides several canard positions and relative angle locations. The fuselage is a simple fairing for wind tunnel mounting with no inlet or cockpit representations, and the lifting surface/body junctions are not filleted or faired in.

The coordinate system used for the model is referenced to the trailing edge of the wing tip. The wing tip location (x, y, z) is defined in this study as (0, -3, 0) in inches. The model is at the 11 degree angle-of-attack with the airstream. The canard is positioned co-planar with the wing and at 0 degrees angle-of-attack with the body centerline, as is the wing.

The data taken in this study contains velocity and pressure information from a series of data points in planes which have their unit normals parallel to the freestream velocity vector (and wind tunnel centerline); their relative locations are shown in Figure 8. The data points are probed at 100 point sets. At each point the values of flow angularity, velocity, and pressure coefficients are developed in real time, using the seven port pressure values and fourth order calibration polynomials. The reduced results are stored on disk for further examination.

For this data, the wind tunnel airspeed was set at 100 fps. The model was suspended from the test section ceiling, without splitter plate, at the 11 degree angle-of-attack setting.

11

III. Results Summary

A. General Flow Characteristics

The model developed flow characteristics typical of sharp leading edge lifting surface configurations. Both the wing and canard exhibited leading edge separation vorticity as well as tip vorticity. In the discussions below, these characteristics are shown graphically in different ways, with the intent of indicating their streamwise development. This is shown by presentations, in progressive streamwise locations, of planar data with these data planes perpendicular to the free stream flow.

The pressure data contained graphically in this document is ΔC_{P_O}, the difference in total pressure between that seen locally at the probe tip and that of the freestream pressure. It is also normalized to freestream dynamic pressure.

$$\Delta C_{P_o} \approx \frac{P_{oL} - P_o}{P_o - P_\infty} \qquad (1)$$

Thus the plotted values represent the difference between local total pressure P_{oL} and freestream total pressure P_o that has been normalized by the difference in freestream total pressure and free stream static pressure P_∞.

With this data representation as the value of ΔC_{P_o} becomes increasingly negative, the local total pressure drops, indicating an energy loss. Thus, as data points move into the freestream the plots should indicate a trend to zero values for ΔC_{P_o} .

12

The raw probe pressure data is converted to pressure and velocity values by interpretation of pressure differences at the seven ports; this requires probe calibration in uniform flow. When large velocity gradients in the flow to be measured are encountered, such as a shear layer or boundary layer, incorrect interpretation of probe pressures can result. These errors are due to the finite diameter of the probe and the spacing of the outer ring of ports. Flow direction can be misinterpreted because velocity gradients may indicate different but parallel flow velocity vectors seen at the probe ports. This could be interpreted, for example, as uniform flow at an angle to the probe rather than parallel flow with large velocity gradients. Therefore, pressure and velocity data inside the shear layers of concentrated vorticity should be interpreted as qualitative and not quantitative. Thus, the location of these disturbances can be properly documented, but absolute values of pressure and velocity should be suspect when generated internally to their strong shear layers.

Graphically obvious examples of this are the total pressure coefficients quoted at some locations in the wing tip vorticity. On the fuselage side of these vortices some of the values of ΔC_{Po} are positive. Because this study was done using isentropic flow, an increase in local total pressure over freestream total pressure is impossible. What has happened is misinterpretation of port pressure by the computerized calibration equations. The large velocity gradients required to bring the cross velocity

13

field from spanwise flow outside the immediate tip vortex region to a crossflow direction into the wing upper surface consistent with the vortex flow do not allow a uniform flow field over the finite tip of the probe.

In the outer reaches of the vortex, the over prediction of local total pressure overshadows the slight actual loss in total pressure due to viscosity effects in the vortex shear layers. A fictitious increase in ΔC_{Po} is predicted. This wake disturbance is there, but some of the calculated pressure values found in this disturbance are unrealistic. The location for the phenomenon is predicted, but the absolute values for some of the pressures are not correct. Therefore, at these locations the pressure data must be ignored. As smaller probes are developed, this diameter sensitivity will be reduced.

Along with the ΔC_{Po} values presented in graphical form in the data of the report, several other data items are available from the probe for each point in the flow field including nondimensionalized coefficients of dynamic and static pressure. These definitions are similar to that of ΔC_{Po}.

$$\Delta C_{P_{static}} = \frac{P_{\infty_L} - P_{\infty}}{P_O - P_{\infty}} \tag{2}$$

$$\Delta C_{P_{dynamic}} = \Delta C_{Po} - \Delta C_{P_{static}} \tag{3}$$

14

Also available from the probe is cross velocity information, with the velocity components u and v representing total velocity in the x and y directions, respectively.

$$u = \frac{Vx}{V_\infty} \text{local}$$

$$v = \frac{Vy}{V_\infty} \text{local}$$

(4)

The sign sense is of the coordinate system used throughout the report.

The test results in the graphical data of the report are organized and presented below by constant streamwise location data planes, with the plane most upstream presented first. The test results are for three basic model configurations. The body alone was tested first, then the wing was added to the body for a series of tests, and finally, a detailed examination was made of the wing, body, and canard combination. The results are organized in this order.

Interpretation of the graphical results presented in the following sections can be facilitated by considering Figures 9 and 10. These figures illustrate the position of a typical data plane (streamwise station 4) relative to the wind tunnel model. In Figure 9 the data plane and its location relative to the wind tunnel model is represented by the metal plate next to the model. This model is mounted on the tunnel ceiling at 11 degrees angle-of-attack to the freestream direction. The plate is located on the low pressure side of the lifting surfaces as are the data planes for the wake maps.

15

On the metal plate is a total pressure coefficient contour plot for streamwise station 4. This plot contains the same data that is in the data set for the 4 inch streamwise location of the Wing/Body/Canard section. Note that this data plane is just aft of the canard trailing edge and passes through only the outboard and forward most areas of the wing. Figure 10 shows a streamwise (looking downstream in the -z direction) view of the data plots in this example data plane. The cross velocity vectors appear on the left and total pressure coefficient contours on the right. The model spanwise direction corresponds to the negative y direction for the data. The model lift direction corresponds to the positive x direction. The model drag direction corresponds to the negative z direction.

The wake data for this plane illustrates most of the major characteristics seen in the other data planes. Note that on the wing the inboard vorticity is that of the leading edge separation vortex, while the tip vortex is depicted at the wing tip. The canard wake is shown just downstream of the canard trailing edge and can be seen in the figure near the body in the total pressure contour plot. The canard leading edge is aft swept. Therefore, the canard leading edge separation vortex sheds off the canard close to its tip. The data planes intersect this vortex in such a way that the cross velocity vectors indicate a positive rotation component about the z axis. The canard tip and leading edge separation vorticity combine in an additive fashion to show the

16

large vorticity concentration at the canard tip station in Figure 9.

The data plane and relative model locations are similar for the other data planes. In all cases (Body, Wing/Body, Wing/Body/Canard) a coordinate origin is defined at some convenient point with z parallel to V_∞. Therefore, some geometric model characteristics such as the local wing tip will change with variations in streamwise locations of the data planes because the model is at an 11 degree angle with respect to the freestream velocity direction.

B. Body Only

An initial set of data was taken with the body alone and mounted next to tunnel ceiling. Since no provision was made for the Wing/Body/Canard tests to move the body outside the wind tunnel boundary layer, a brief check of the body alone using this mounting technique was made. Since the wing was not present to establish a reference point, the origin for the coordinate system used for the body alone tests was established at a surface point directly below the body centerline and aft of the nose.

In Figures B1 - B5, a series of data planes in streamwise increments of 2 inches are presented from streamwise location 0 in Figure B1, to streamwise location -8 inches in Figure B5. These figures describe the local cross velocity fields about the body at the 11 degree angle-of-attack. Note the similar nature of these flow patterns. From the surface, the crossflow shows the

17

flow from the body surface at its centerline to a y value of -6
inches and the velocity drift is caused by the body being at an
angle-of-attack. Note that very close to the body surface (y=0) a
significant flow upwards into the tunnel ceiling is created by
the presence of the corner of the body. This body corner is
forcing flow to travel parallel to the body surface, giving the
crossflow the orientation shown. The invariance of the flow field
streamwise suggests that nothing unusual is happening to the flow
due to this particular body.

C. Wing/Body Results

After the body-only flow surveys were taken, a series of
surveys were taken with just the wing mounted on the body. This
should provide basic forward-swept wing characteristics that can
later be compared with those taken from the wing in the wake of
the canard. For these flow surveys, an origin for the coordinate
system was chosen at 3 inches inboard of the trailing edge tip of
the wing. Therefore, in the following plots a positive x implies
a movement away from the upper surface (low pressure side) of the
port wing in a direction perpendicular to the free stream
velocity vector and parallel to the wind tunnel floor. A positive
y direction implies a direction inboard from the wing tip toward
the wing root -- parallel to the vertical side walls of the wind
tunnel. A positive z movement is upstream parallel to the free
stream direction.

18

1. Streamwise Station 0

In Figure WB1, the cross velocity vectors are plotted for the streamwise station 0. Two concentrated areas of streamwise vorticity are indicated, one vortex near the wing leading edge and one at the wing tip. The wing leading edge intersects this plane approximately 4.5 inches inboard of the origin. Since the projection of the vortex origin near the wing leading edge is approximately 2.5 inches inboard of this edge, a shift downstream of the leading edge vortex has occurred. This vortex moves inboard at a slightly higher angle than the leading edge sweep would indicate. Due to the geometry of the wing in the data plane, he leading edge vortex appears closer to the origir than the wing leading edge. Note that the clockwise rotation in the data plane is consistent with a detachment and reattachment of the flow due to the sharp leading edge separation bubble.

The wing tip vortex is the stronger vortex at this streamwise location. The wing trailing edge tip is located at $y = -3$ inches, and a strong vortex is shown there with the proper counter clockwise rotation. Axonometric plots are made of ΔC_{P_o} for this data plane in Figures WB2 - WB4. Again, the x and y coordinates are data plane coordinates with ΔC_{P_o} plotted along the third dimension. Figure WB4 is presented to illustrate the relative magnitudes of these changes in ΔC_{P_o}. For this wing geometry, note the relative amounts of energy loss in the leading edge separation region as opposed to those of the tip. While the cross velocity plots show only the velocity vector projections in

19

the x-y plane, the ΔC_{Po} plots show total relative magnitudes, and the leading edge separation region appears to dissipate much more energy than the tip region.

Figure WB5 presents lines of constant ΔC_{Po} in the x-y plane that corresponds to the cross velocity plot of WB1. By comparing these figures, the correlation between cross velocity vectors and ΔC_{Po} contours can be seen. The ΔC_{Po} contours identify the "core" of the vorticity and, as will be shown in later figures, can identify multiple cores in a single large system of vorticity. Note that as the line spacing narrows, larger gradients of ΔC_{Po} are implied and correlate with the steep slopes on the axonometric plots.

2. Streamwise Station -4

Figures WB6 - WB10 present the data for streamwise station -4. At this station the wing intersects the data plane at the wing root, located at y = 9.8 inches and its trailing edge at y = 0.8 inches. The tip vortex is indicated at about -2.8 inches in the y direction and about 0.6 inches in the x direction. The relative lengths of the cross velocity vectors indicate that the tip vortex system is approximately equal in strength to the leading edge vortex. In Figure WB6 the area of the data plane outboard of y = -0.8 inches is in the freestream and contains a wake signature from the upstream wing trailing edge. This figure also shows the cross velocity vectors with two major systems of vorticity. Note that the rotational sense of these two vortex

20

systems tends to impart a downwash onto the wing's upper surface. The leading edge vortex has a projection on this plane that indicates a vortex core location at about 6 inches on the y axis and .75 inches on the x axis. This vortex system has become almost a streamwise vortex system at this point downstream on the model.

The axonometric plots for streamwise station -4 show the large energy dissipation region of the leading edge vortex with a much smaller region at the wing tip. Careful examination of Figure WB8 shows the wake shed from the wing trailing edge at y coordinates of less than 1 inch.

The wake can be better seen in the narrow range ΔC_{p_0} contour plot of Figure WB10. Note the concentration of ΔC_{p_0} loss in the region around and slightly above the tip vortex. Due to geometry limitations of the present probe positioning system, the probe could not be moved to any values more negative in x than those shown. Near the wing leading edge junction with this data plane, at 9 inches in y, the leading edge separation vortex formation indicates multiple core vortex locations.

3. Streamwise Station -8

This data plane resides 8 inches downstream of the wing tip trailing edge. The wing intersects the plane at a y value of 1.6 inches. The area outboard of this location is contained only in the freestream wing wake. The cross velocity vectors of this plane in Figure WB11 indicate that the vorticity

21

from the leading edge separation flow has moved inboard. The tip vortex is moving downstream at the same x-y location from which it was generated. The velocity field in between these vortex systems appears stronger now that most of the wing is upstream of this data plane. The strength of the tip vortex has not decreased much, but the leading edge separation cross velocity field appears to be weaker.

The axonometric plots of Figures WB12 - WB14 show the wing wake clearly, especially Figure WB13. In this figure the ridge of ΔC_{Po} from just behind the wing and data plane intersection, at about y = 2 inches, to the tip vortex system is the wing wake. Note that its signature of ΔC_{Po} loss, though smaller than concentrations of viscous loss due to vorticity, is still measurable with the seven-hole probe.

In Figure WB15 a ΔC_{Po} contour plot of -0.02 to -0.4 in identifies the wing wake and areas of concentration vorticity. Note that the wake appears to "curl up" into the vortex region downstream from the wing tip. Using this range of ΔC_{Po} , a small part of the leading edge separation vortex is visible near the y = 6 inches region on the y axis. Only a hint of the tip vortex is visible, showing that these concentrations of ΔC_{Po} require a wider ΔC_{Po} range in plotting and have had relatively stronger mechanisms for energy loss.

D. Wing/Body/Canard Results

22

The data format for the wing/body/canard is similar to that of the wing/body. It presents as the first plot the cross velocity vectors for the entire sampled data plane at a particular streamwise station. This region is bounded by the low pressure side of the lifting surfaces, the body, and the largest spanwise locations necessary to capture all of the relevant flow characteristics. The second set of plots contains axonometric presentations of the loss in total pressure over the same region that contained the crossflow velocity vectors. Several viewing orientations of "look angles" are presented for each plane of data so that each major characteristic can be observed. There is also a final plot that presents relative magnitudes of total pressure losses to demonstrate relative disturbance strengths. Following the axonometric plots are contour plots of total pressure losses. With these plots, locations of wake and vortex filaments can be determined. With these general locations defined by these plots, pressure and velocity numbers can be obtained from the Appendix listings for particular points of interest.

1. Streamwise Station 9

The most upstream location used to take data for the wing/body/canard is 9 inches upstream from the trailing edge wing tip, as noted in Figure 8. This plane intersects the leading edge of the canard at y = 3.9 inches or about two-thirds of the way from the canard root to the tip. Recall that the coordinate origin is still the trailing edge tip of the wing.

23

In Figure WBC1 the cross velocity vector plot shows basically a single rotational velocity disturbance. This disturbance exists at the leading edge of the canard, providing a rotation that is consistent with a leading edge separation vortex. Note that this vortex region is essentially parallel to the leading edge. Therefore, the cross velocity plot in a streamwise constant plane does not present the full rotational strength of this strong vortex. This would be available only in a plane that is perpendicular to the axis of rotation of the vortex core. Since this plane is upstream of the canard tip, the only vortex system indicated is that due to the leading edge separation.

Figures WBC2 - WBC4 present axonometric plots of ΔC_{P_o} which show the large energy dissipation region in the vortex. Note that the region near the fuselage junction with the canard at $y = 9.8$ inches indicates losses in total pressure due to the canard fuselage interaction at that junction.

Figure WBC5 presents a contour plot of ΔC_{P_o} which shows the leading edge separation vortex centered about 5.8 inches on the y axis up from the origin. The leading edge of the canard in this plane is at $y = 3.9$ inches. There is a tight concentration of ΔC_{P_o} loss at this leading edge point, with a wake-like distribution from the leading edge up over to the vortex concentration from the upstream separation.

2. Streamwise Station 4

24

Figures WBC6 - WBC10 present data from the plane located 4 inches upstream of the origin. This plane falls just downstream from the canard with the wing and data plane intersection lying between -.6 inches and -.3 inches on the y axis. This data plane is unique in this data set in that the entire wake from thhe canard is in the free stream. At this point in the flow, the canard leading edge separation vortex has turned streamwise. Its location is essentially that of the tip vortex of the canard, and the two regions of vorticity meld into one system.

In Figure WBC6 the cross velocity plot shows three areas of vorticity. The largest is the canard leading edge separation and tip vortices centered at 3 inches on the y axis. The leading edge separation of the wing creates the vortex system centered at $y = -1$ inch with the tip producing the vorticity at $y = -3$ inches. Note that the wing leading edge is swept forward. The resulting vortex core of its separation vortex is oriented so that the velocity components of this plane specify a clockwise rotation on the data plane, rather than the counter-clockwise sense of the canard leading edge separation vortex.

The downwash due to the canard is in the negative x direction with a transition to the vortex flow close to the canard vortex core. The downwash on the wing from the wing leading edge vortex and tip vortex is also in the negative x direction. The overall cross velocity flow at this streamwise location seems to be dominated by the canard wake.

25

The axonometric plots of Figures WBC7 - WBC9 show the vorticity regions of ΔC_{Po} plus the trailing edge signature in ΔC_{Po} of the canard wake. The canard tip vortex is the most prominent region of ΔC_{Po} . The large region of dissipation contains remnants of both the leading edge separation and tip vorticity. Inboard of this region is the canard wake, especially visible in Figure WBC7. The ridge in ΔC_{Po} less inboard of the canard tip vorticity is the signature of canard wake in free stream flow. The concentration of loss at the fuselage boundary is the fuselage canard wake interaction. Note that the region just outboard of the canard tip vorticity is freestream and has correspondingly no ΔC_{Po} signature. This region should not have a wake since it is outboard of the canard tip, but in front of the wing.

Two areas of concentrated vorticity exist outboard of the above characteristics. These correspond to the wing tip vorticity (the most outboard) and the leading edge separation vortex (the most inboard). Note that the leading edge separation appears to absorb much more energy than the wing tip region.

In Figure WBC10 a contour plot of ΔC_{Po} using ΔC_{Po} range of -.025 to -0.5 is shown. This range clearly shows the fuselage junction with the canard wake, the canard wake, and the canard tip vortex region. The leading edge and tip vorticity of the wing are formed more outboard. The wrap-up of the canard wake into the canard tip vorticity can be seen, and its relative strength compared to the vortex is apparent.

26

3. Streamwise Station 2

This next data plane is 2 inches upstream from the coordinate origin. This plane again is downstream of the canard with the wing leading edge intersecting at 1.8 inches on the y axis. The wing intersection terminates at the wing tip.

The cross velocity plot of Figure WBC11 shows a complicated circulation system in an area of the y axis at approximately y = 3 inches. This area contains the downstream remains of the canard leading edge and tip vorticity. Interactions are taking place here between this canard vorticity and the wing leading edge separation vorticity located approximately at the y = 1 inch position. Note that due to their counter-rotational sense, the downwash between them is now in the positive x direction, with significant velocities induced there due to the reinforcement in cross velocity influence by both regions of vorticity.

The wing tip vortex is clearly visible at y = -3 inches, with the correct rotational sense demonstrated. The effect of no flow penetration at the wing surface is seen in the downwash between the wing leading edge and tip vorticity. Here an inboard spanwise flow is developed along the surface of the wing.

The axonometric plots of Figures WBC12 - WBC14 show the relative magnitudes of the regions of ΔC_{P_o}. Note that the canard wake signature is not apparent between the fuselage interaction and the canard vorticity. The wake appears to have moved in the negative x direction in response to the downwash field. Due to

27

the probe geometry it could not be moved far enough in the
negative x direction to find the canard wake.

The canard vorticity shows the concentrations at the
remnants of the cores of the original constituents. The proximity
of the canard vorticity to the leading edge vorticity is shown to
be close. Note that the dissipation in the wing leading edge
separation vortex is much stronger than in any other vortex
system in this plane. The wing tip vorticity is much weaker.
Contour plots of ΔC_{Po} in Figure WBC15 show the relative locations
of the areas of concentrated vorticity. Note the large region
located near x = 2 inches running from 1 to 6 inches on the y
axis. This is the canard vorticity. The wing leading edge
separation vortex, while possessing opposite rotational sense,
has moved close to the canard vorticity. This spanwise movement
is dictated by the leading sweep geometry of the sharp leading
edge creating this vortex. The wing tip vorticity remains at the
tip as a much weaker region of ΔC_{Po}.

4. Streamwise Station 0

On the data plane at streamwise station 0, the wing
intersects in the most inboard fashion at its leading edge
located at 4.3 inches on the y axis. The tip is the most outboard
point in common between the wing and the data plane.

The concentrations of vorticity in this plane shown by cross
velocity vectors are presented in Figure WBC16. Due to the
geometry of the swept leading edge, the leading separation vortex

28

continues to move inboard as the data planes move downstream. In this data plane the leading edge separation vortex now centers at approximately y = 2 inches. With the canard system centered on the y = 3 inches point, a strong interaction occurs, which is visible in the large magnitude cross velocity vectors lying between the two vortex systems. The combination of flow effects of the canard vortex system and the wing tip vortex induces essentially inboard spanwise flow from approximately 2 inches above the upper wing surface. It should be noted that the leading edge separation vortex has not fully re-oriented to a streamwise core at this data plane. Therefore, some of its crossflow velocity influence cannot be seen in the cross velocities of this data plane.

Axonometric plots of this data plane are given in Figures WBC17 - WBC19. The canard wake is again visible from the fuselage interference region to the canard vorticity. The wing leading edge separation vortex has become the dominant mechanism of energy dissipation in this data plane, as shown in Figure WBC19. Also note that the two core constituents to the canard vorticity are still visible as separate characteristic regions of energy loss with proper selecting of plotting range. The contour plots of ΔC_{P_O} in Figure WBC19 show the two cores of vorticity in the canard vortex system. Their x location is about 2.3 inches, but a core is indicated at the y = 4.5 location and another at y = 1.2 inches. Note that this system from the canard appears to be moving upwards and away from the wing as the system travels

29

downstream. This shift may be due to the strength of the wing
leading edge separation vortex just below the canard system,
which is tied to the wing geometry. The shift inboard of the wing
leading edge separation vortex is due to the wing geometry and is
still progressing at this streamwise station. The wing tip
vorticity is at the -3 inch wing tip location on the y axis.

    5. Streamwise Station -2

        In the data plane 2 inches downstream from the origin,
the wing intersects the data plane from the 6.6 inch point
(leading edge) to the -1.8 inch point (trailing edge) on the y
axis. The cross velocity vectors for this data plane can be seen
in Figure WBC21. The canard tip vorticity is centered about 4.2
inches above the x axis while the leading edge vorticity is at
2.5 inches above. The core of the leading edge vorticity has now
begun to turn nearly streamwise. The canard vorticity appears to
be preventing the wing leading edge separation vortex from moving
further inboard. This can be observed when comparing the wing
data with and without canard.

        The wing tip vorticity is aft of the wing tip in the free
stream wake at -3 inches on the y axis. The downwash generated by
this region has a large component in the negative x direction.
The downwash seen inboard of the wing's leading edge is an upwash
and appears to be a function of the leading edge vorticity. Note
that even though the core of the wing leading edge vortex has now
moved away from the wing leading edge and more downstream, the

30

crossflow due to both the canard vorticity and the wing leading edge separation vortex moves the near flow of the wing outboard.

The axonometric plots of Figures WBC22 - WBC24 show the dominance of energy loss in the wing leading edge separation region as compared to the other locations. Note that the wake of the canard is still visible. The wake can be seen stretching from the fuselage interaction disturbance to the large concentration of vorticity in the region just above the wing at y = 3 to 4 inches. Due to the geometry of the probe positioning system, only the beginnings of the wing wake inboard of the tip vorticity are visible. Note also that there still appear to be three distinct cores of vorticity in the region from 0 to 5 inches on the y axis. There is one core near the wing which corresponds to the wing leading edge separation system and there are two lesser cores from the canard. The interaction between the canard vorticity and the wing leading edge separation vortex has caused the cores of the canard system to begin to separate.

The contour plots of Figure WBC25 show these cores more distinctly. However, the cross velocity plot seems to indicate that the canard vorticity crossflow is probably due mainly to that core located at about 4 inches on the y axis and 2 inches on the x axis. A small portion of the wing wake can now be seen next to the wing tip vortex.

6. Streamwise Station -4

31

At this location downstream, the wing intersects the data plane from the y = 9 inch point at the wing leading edge to the -0.7 inch point at the trailing edge. The cross velocity vectors for this data plane are contained in Figure WBC26. The significant effects of the canard wake on the wing flow field can be seen graphically by comparing Figure WBC26 (with canard) and Figure WB6 (without canard). Note the difference in location of the wing leading edge separation vortex. With the canard wake added and its associated concentration of vorticity at y = 4 inches, the leading edge separation vortex is held to 3 inches above the x axis. There is also an added strong downwash on the wing due to the canard effects.

The axonometric plots of Figures WBC27 - WBC28 show the very slight ΔC_{Po} signature of the canard wake as it passes just above the wing inboard of the canard vorticity. Note also the smaller core of ΔC_{Po} loss because the weaker of the two vortex cores from the canard vortex system has been moved below the wing leading edge system and has little signature left in the cross velocity vectors. The shape of the wing leading edge separation vortex energy dissipation region has been flattened due to the near presence of the canard vortex. This reshaping can be seen more easily in the contour plots of Figure WBC30. Note that just a hint of the second core of the canard system is still visible and the primary core of the canard system is modifying the wing leading edge system. It should be pointed out that at this data plane and those downstream, the primary mechanism of leading edge

32

separation has been lost. The wing leading edge separation
signature at this streamwise location is the remnant of an
occurrence upstream and is no longer being generated locally by
the wing leading edge since this separation is not found inboard
of the y = 3 inches region.

7. Streamwise Station -6

At the 6 inch location downstream of the coordinate
system origin, the wing intersection with the data plane begins
at 0.4 inches on the y axis and is continuous inboard to the wing
root. In Figure WBC31 three major regions of vorticity are noted.
The wing tip vortex is at 2.5 inches below the x axis. The now
streamwise-oriented core of vorticity coming from the upstream
leading edge separation of the wing is located about 2.5 inches
above the x axis. The canard vorticity is still at 4 inches above
the x axis. At the wing and fuselage junction, crossflow is
developing due to the simplified geometry of the model. Note the
downwash direction above the wing. The cross velocity indicates a
small drift outboard until just above the wing surface. There the
surface flow appears to be slightly inboard. It should also be
noted that the downwash flow direction is just outboard of the
wing trailing edge. Flow influence from the wing leading edge
separation vorticity quickly gives way to the wing tip vortex
system outboard of it.

The axonometric plots of Figures WBC32 - WBC34 show
concentrated regions of ΔC_{Po} in the same regions suggested by the

33

cross velocity plots. Note that the remnant from the second vortex constituent of the canard vorticity has almost been absorbed by the wing leading edge vortex.

The contour plots in Figure WBC35 are given for a narrow range of ΔC_{Po} to arcentuate the location of the freestream wing wake. Note that at the wing trailing edge location the contours suggest that the wing wake travels outboard to the wing tip vorticity and wraps around the core region of the wing tip vorticity. The large region of energy dissipation above the wing tip vortex corresponds to the canard tip and wing leading edge separation vortex systems.

8. Streamwise Station -8

For the data plane 8 inches downstream of the coordinate origin, the wing intersection with the data plane runs from the wing root to the wing trailing edge at 1.6 inches above the x axis. This is the most downstream plane of data taken. In Figure WBC36 the cross velocity plots indicate that the leading edge separation vortex has almost disappeared as a true vortex. Its influence is the S-shaped reshaping of the crossflow field between the canard vortex system and the wing surface downwash. The downwash just outboard of the wing trailing edge is dominated by outboard velocity components. This data plane can be compared to the wing only configuration shown in Figure WB11.

The axonometric plots of Figures WBC37 - WBC39 show considerable differences in the location and strength of ΔC_{Po}

34

when compared to the plots observed without the canard in Figures
WB12 - WB13. With the canard vorticity to hold it outboard, the
wing leading edge separation vortex does not move inboard to
combine with the wing/fuselage junction losses. In Figure WBC39
the wing wake still can be seen at about the same location with
or without the canard. Again, a narrow range of ΔC_{P_O} is used to
accentuate the wing wake.

IV.   Conclusions

This test data demonstrates that it is possible to locate
the wakes of lifting surfaces in the freestream. For example, in
the data for streamwise station -4, the contours of total
pressure loss, plotted spatially as in Figure WBC10, locate the
exact position of the canard wake. Therefore, the ability to
define experimentally these wake locations has now been
established. Other related test data has shown that the wake
signature in the total pressure can be observed for much smaller
models with zero angle-of-attack. This suggests that even for
small surfaces that are not creating significant airloads the
wake signature is discernable using the seven-hole probe.

Vortical flow can also be observed. The energy losses in the
flow due to viscous effects can be observed in total pressure
loss, allowing documentation of the locations of vorticity. The
tip vorticity for all the lifting surfaces has been observed. The
increasingly stronger velocity gradients dissipate more energy as
the core is approached and appear as larger and larger losses in

35

total pressure. Other test data show that these contours disappear when the lifting surface is brought to a no lift orientation. Leading edge separation vorticity has also been documented using the seven-hole probe, both on forward swept and aft swept surfaces. Its movement spanwise is consistent with the leading edge sweep, and its interaction with other wake flow fields such as the canard vorticity has been observed.

With the above capability to document the wake characteristics of lifting surfaces, several observations can be made about the canard wake, the wing wake, and their effect on each other. The canard wake contains strong rotational flow with significant total pressure loss in the region aft of the tip. This local region contains both the canard tip vortex and the canard leading edge separation vortex, with both rotational flows being in the same rotary direction. The planar region aft of the canard over which significant crossflow exists is relatively large. The resulting canard leading edge separation and tip vortex combination is not tightly knit, but rather loosely spread out. However, this vortex combination represents the strongest single wake characteristic of either the wing or canard.

A different system of rotational flow exists aft of the wing. The wing tip pressure recovery rotational flow is in the same rotary direction as that of the canard tip. However, with the negative leading edge sweep of the wing, the leading edge separation vortex is oriented differently from the aft swept canard leading edge separation vortex. This wing leading edge

36

separation vortex now moves inboard as it moves downstream with the wing leading edge and its rotational component streamwise has a rotary sense opposite to that of the wing tip vortex. When this swept vortex becomes oriented streamwise and trails off downstream, it is near the fuselage and not the tip. The wing wake connects the tip vortex of appropriate rotational sense to a counter-rotational vortex near the fuselage. This counter-rotational vortex is created by the leading edge separation bubble.

As a consequence of the canard and wing geometry of this model, the canard tip vortex and the wing leading edge separation vortex occupy approximately the same spanwise location, with the canard vortex being slightly above the wing planform due to the model's angle-of-attack. Their rotations, however, are in opposite directions and each had significant effects on the other.

The canard tip vorticity appears to stop the inboard movement of the counter rotating wing leading edge vorticity, and force it to turn downstream prematurely. Inboard of that point, no separation is observed. The downwash velocity vectors inboard of the canard tip vorticity imply that the canard wake is forcing the flow on the wing upper surface to stay attached. The sensitivity of this flow adjustment to geometric factors such as canard and wing spacing and relative angles-of-attack has not been examined, but the ability to control the position of the

leading edge separation vortex appears to depend most heavily on the canard span measurement.

The leading edge separation vortex phenomenon has its effect on the canard tip vorticity. The canard tip vorticity appears to be made up of two separate cores, one from the canard tip pressure recovery and a stronger one from the canard leading edge separation. When brought in the presence of the counter rotating but strong wing leading edge separation vortex, the two cores are pulled apart. The weaker core from the tip pressure recovery is quickly overcome, with little or no cross velocity influence detected from it by streamwise station -8.

Using this simple generic forward swept wing model, the wakes of the lifting surfaces and their major flow characteristics have been documented. The flow details of major interest have been included in the graphical summaries presented here for easy comparisons. Future experiments will document flows from both simple models and detailed representations of the forward swept wing demonstrator aircraft.

References

1. Gerner, A.A. and Maurer, C.L., "Calibration of Seven-Hole Probes Suitable for High Angles and Subsonic Compressable Flow," Aeronautics Digest, USAFA-TR-81-4, USAF Academy, May 1981.

2. Clancy, L.J., Aerodynamics, John Wiley and Sons, 1975.

3. Crandall, R., and Sisson, G., "Canard Wake Measurement and Description," _Aeronautics Digest_, USAFA-TR-81-4, USAF Academy, May 1981.

4. "Subsonic and Trisonic Wind Tunnel Facilities Handbook," Department of Aeronautics, USAF Academy, 1979.

Figure 1.   Generic Forward-Swept Wind Tunnel Model
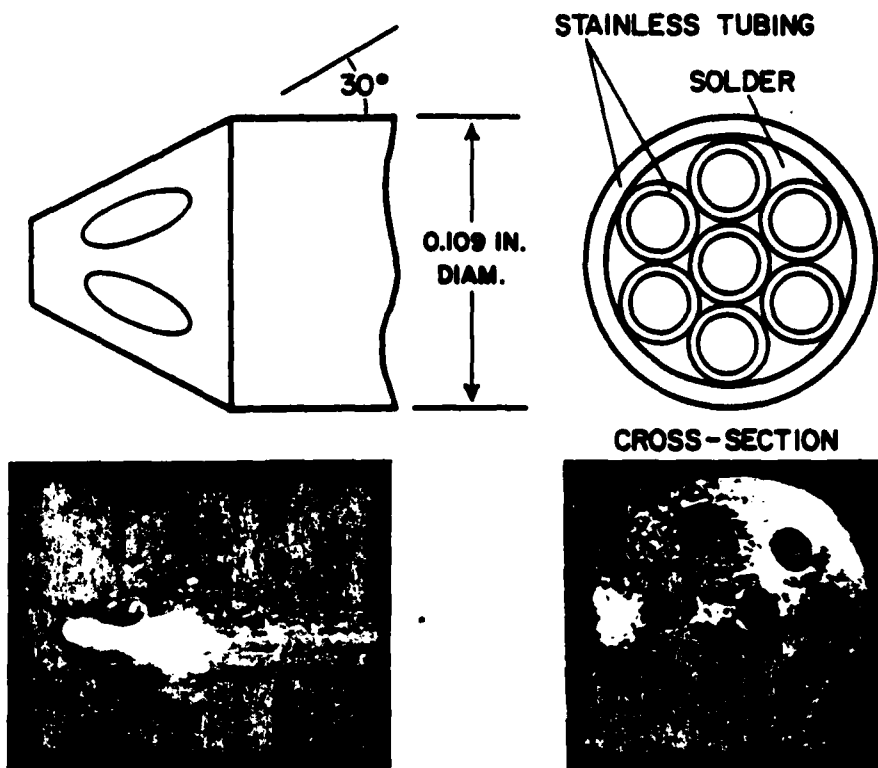
Figure 2.   Seven-Hole Pressure Probe
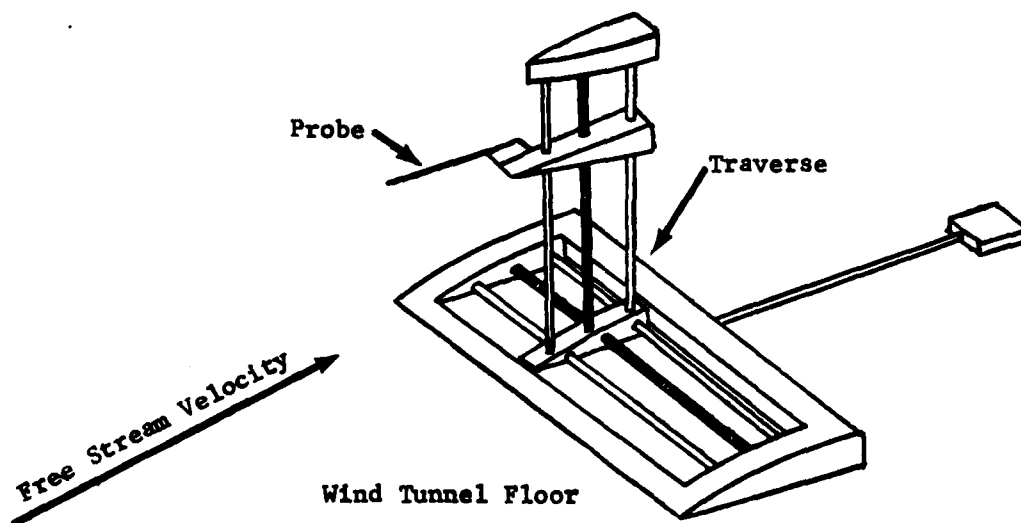
Figure 3.   Seven-Hole Probe Positioning Traverse

41
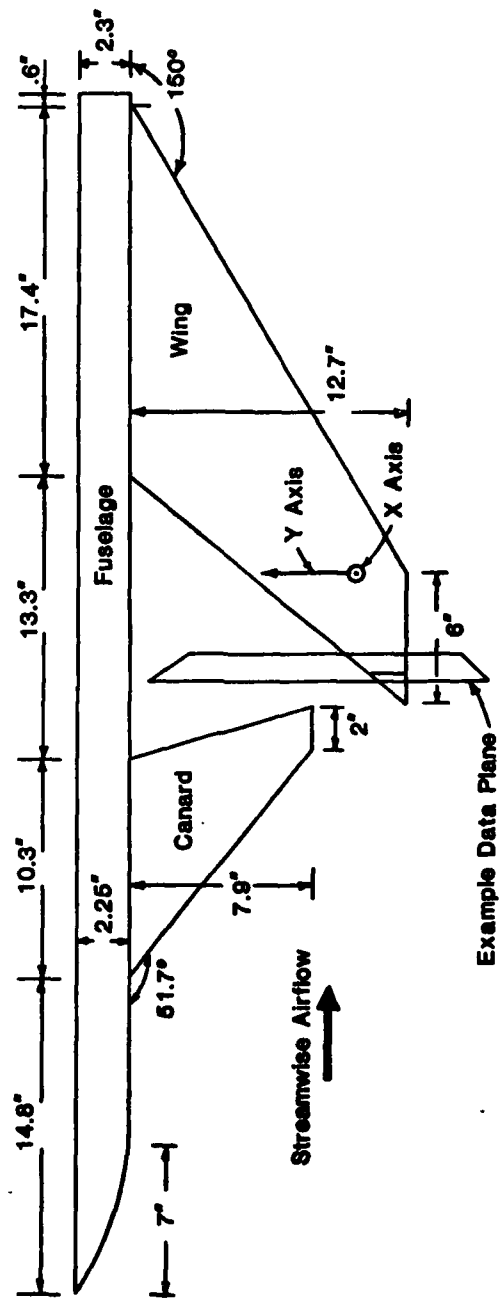
igure 4.   Wind Tunnel Model and Coordinate Axis as Mounted
in the Wind Tunnel

42
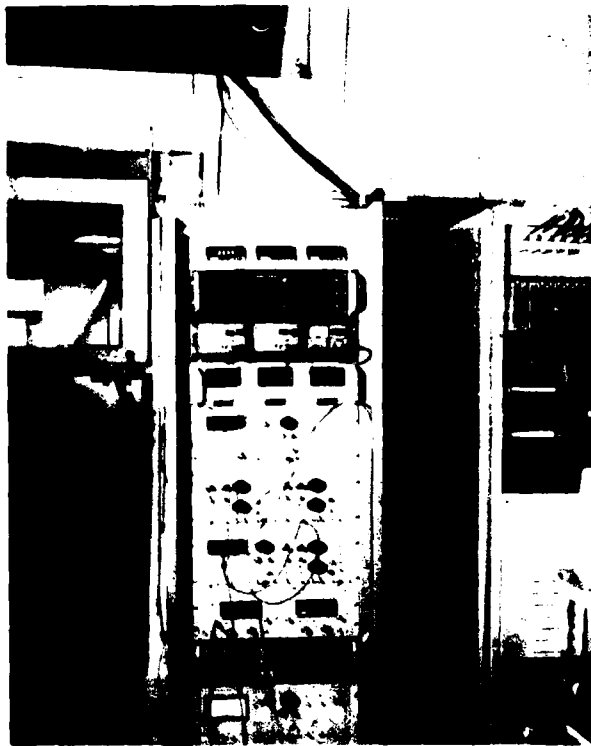
Figure 5. Probe Positioning and Pressure Data Gathering
Equipment

Figure 6. Computer and Disk Drives for Data Reduction and
Management

43
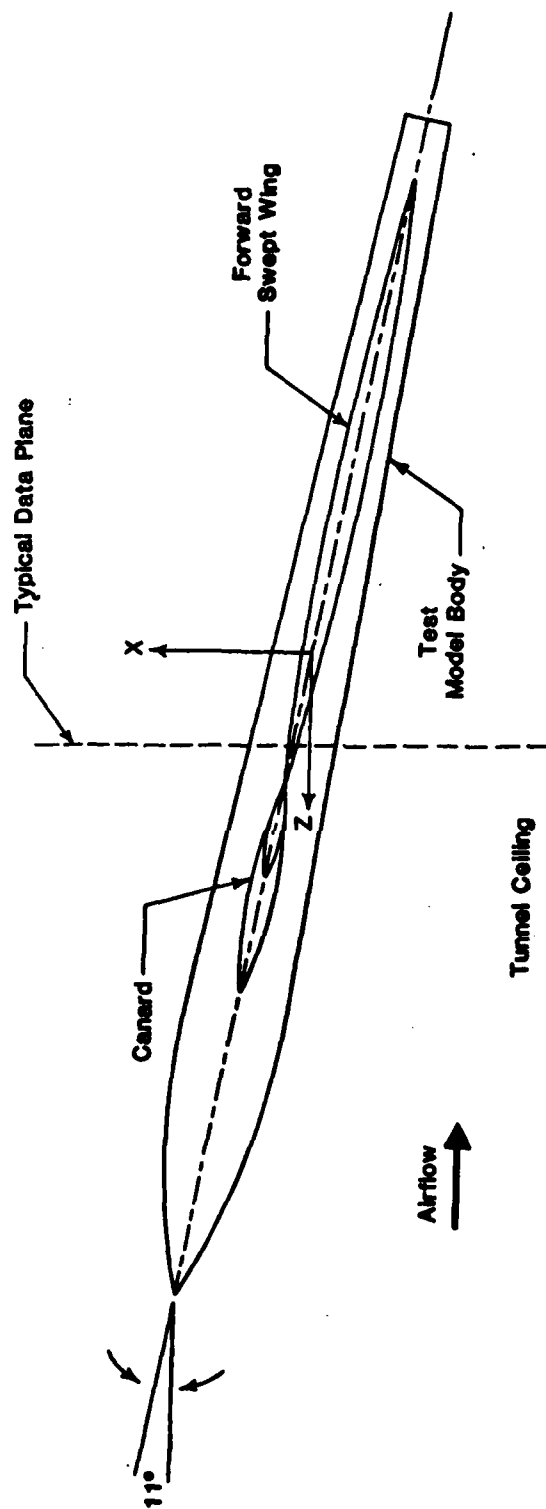
Figure 7. Wind Tunnel Model as Seen by Viewing Upwards
(Positive y Direction) from the Wind Tunnel
Floor

44
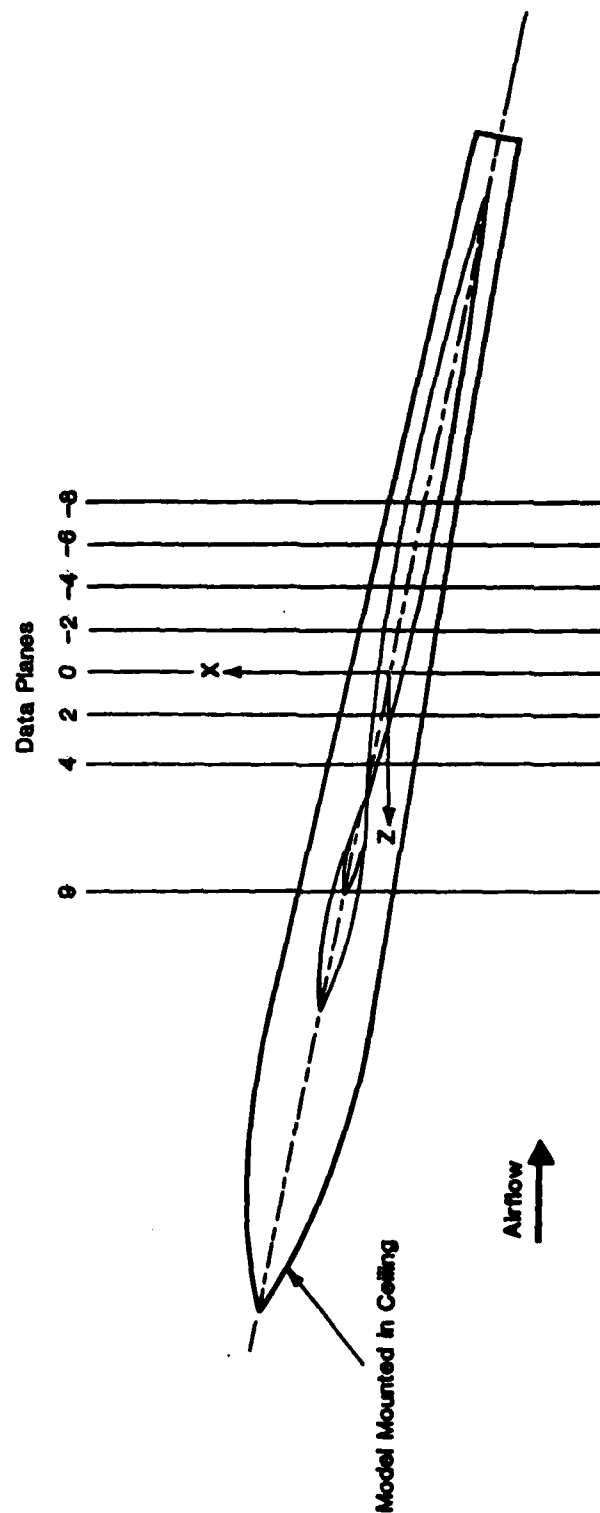
Figure 8. Data Plane Locations Relative to Model for Wing and Wing Body

Figure 9.   Wind Tunnel Model and Typical Data Plane

(Pressure)

(Velocity)

Figure 10. Typical Velocity and Pressure Data Plane Location
Relative to Model

47
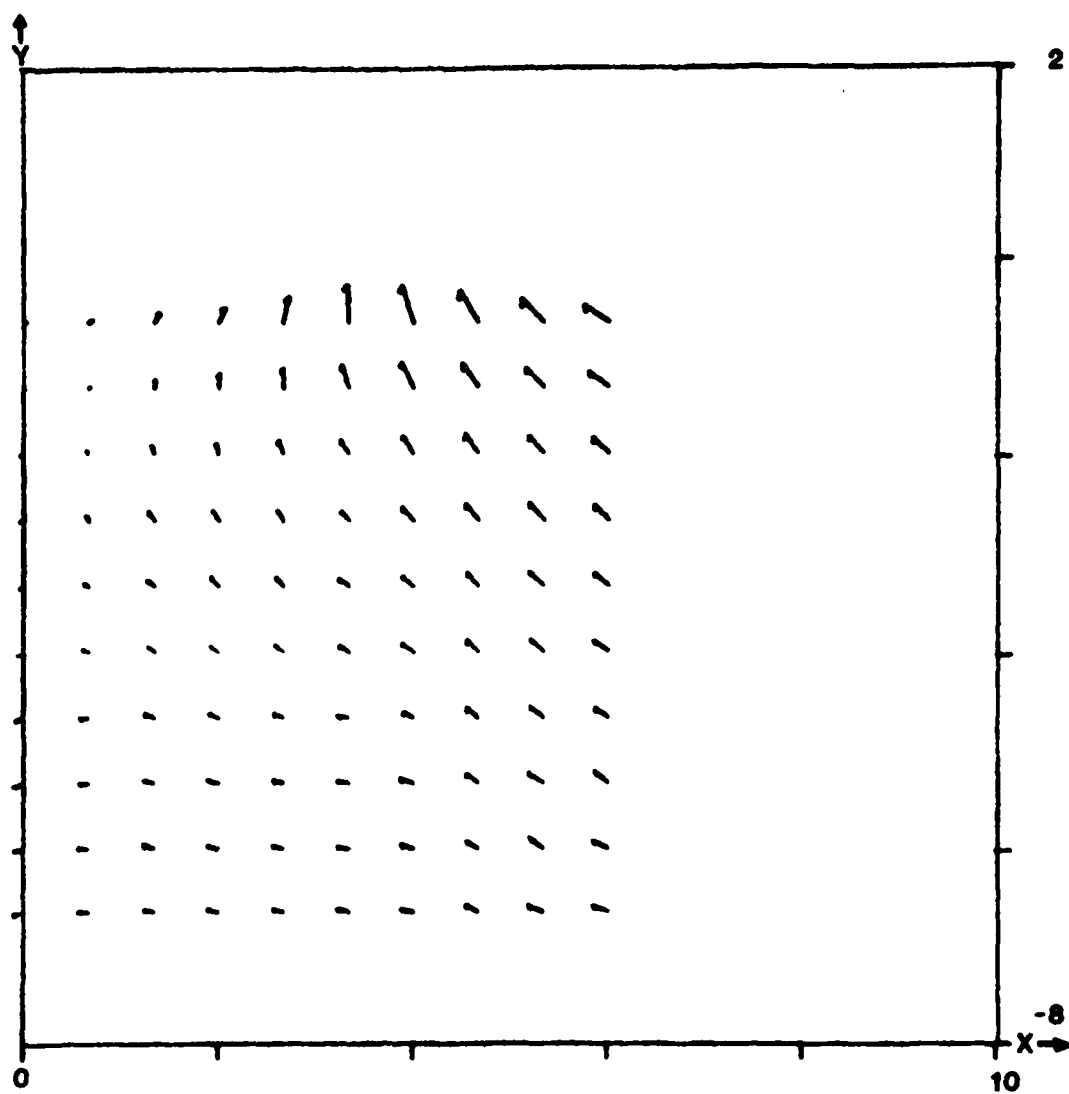
Figure B1. Cross Velocity Field for Streamwise Station 0

48
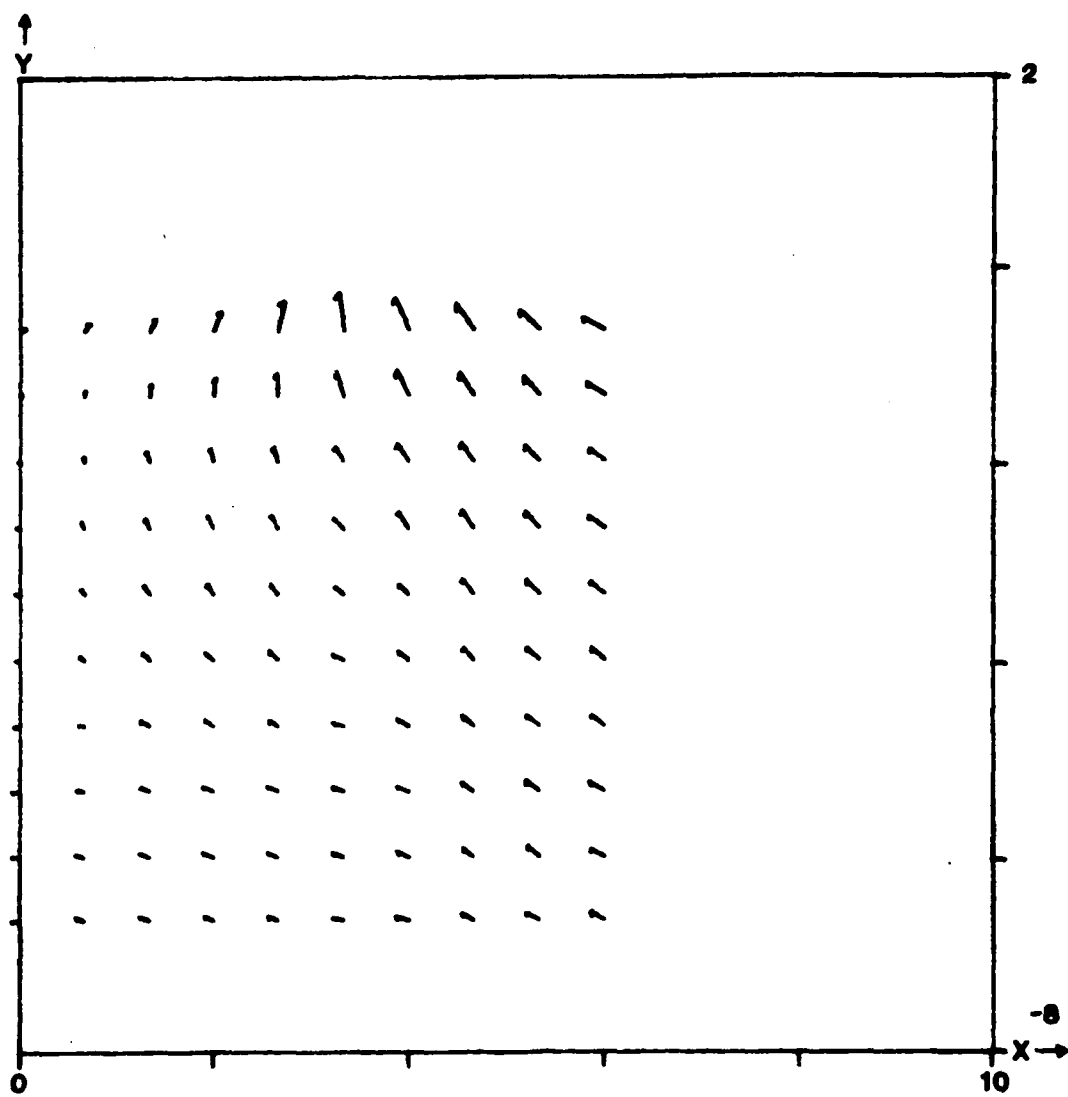
Figure B2. Cross Velocity Field for Streamwise Station -2

49
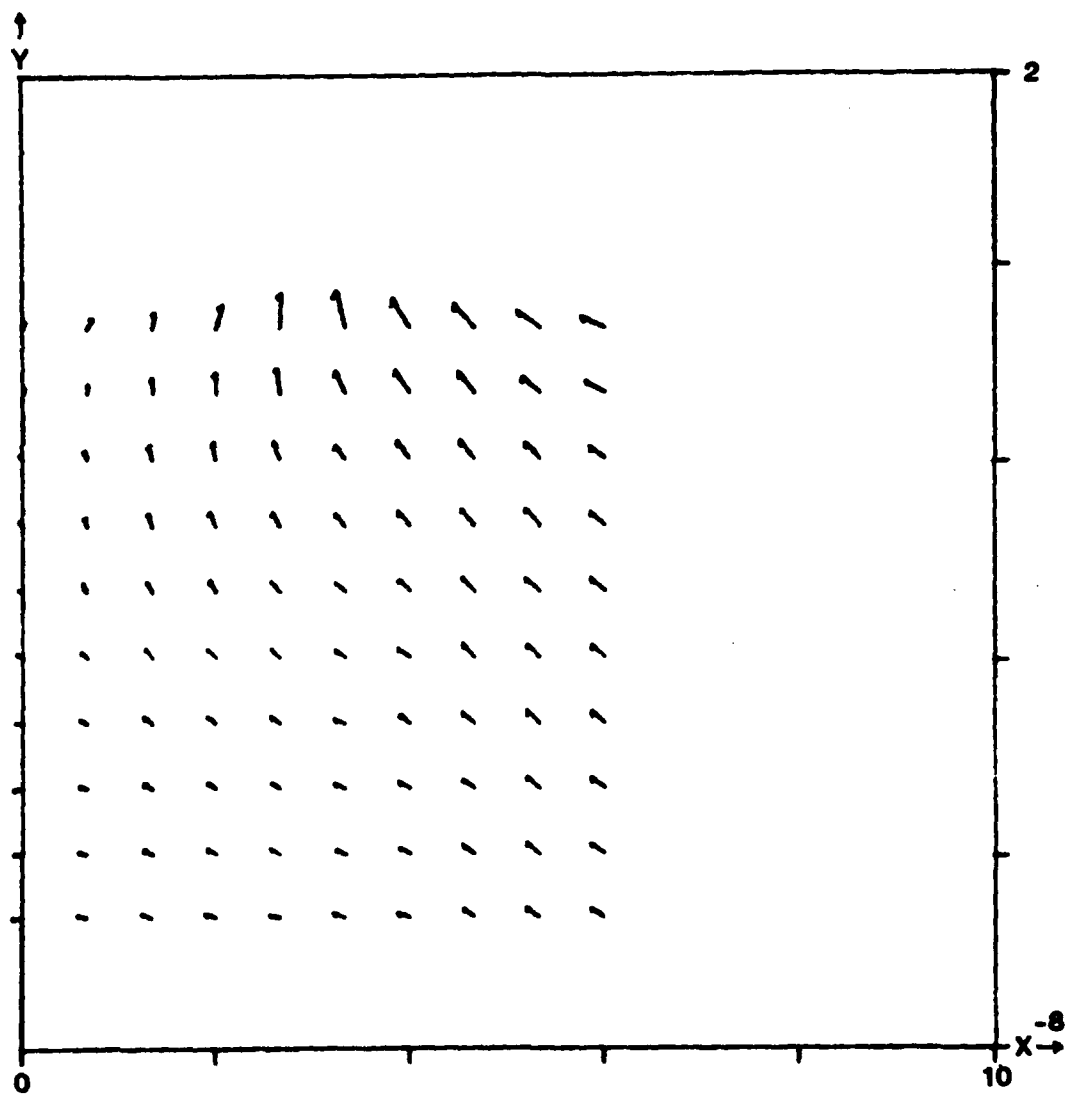
Figure B3.   Cross Velocity Field for Streamwise Station -4

50
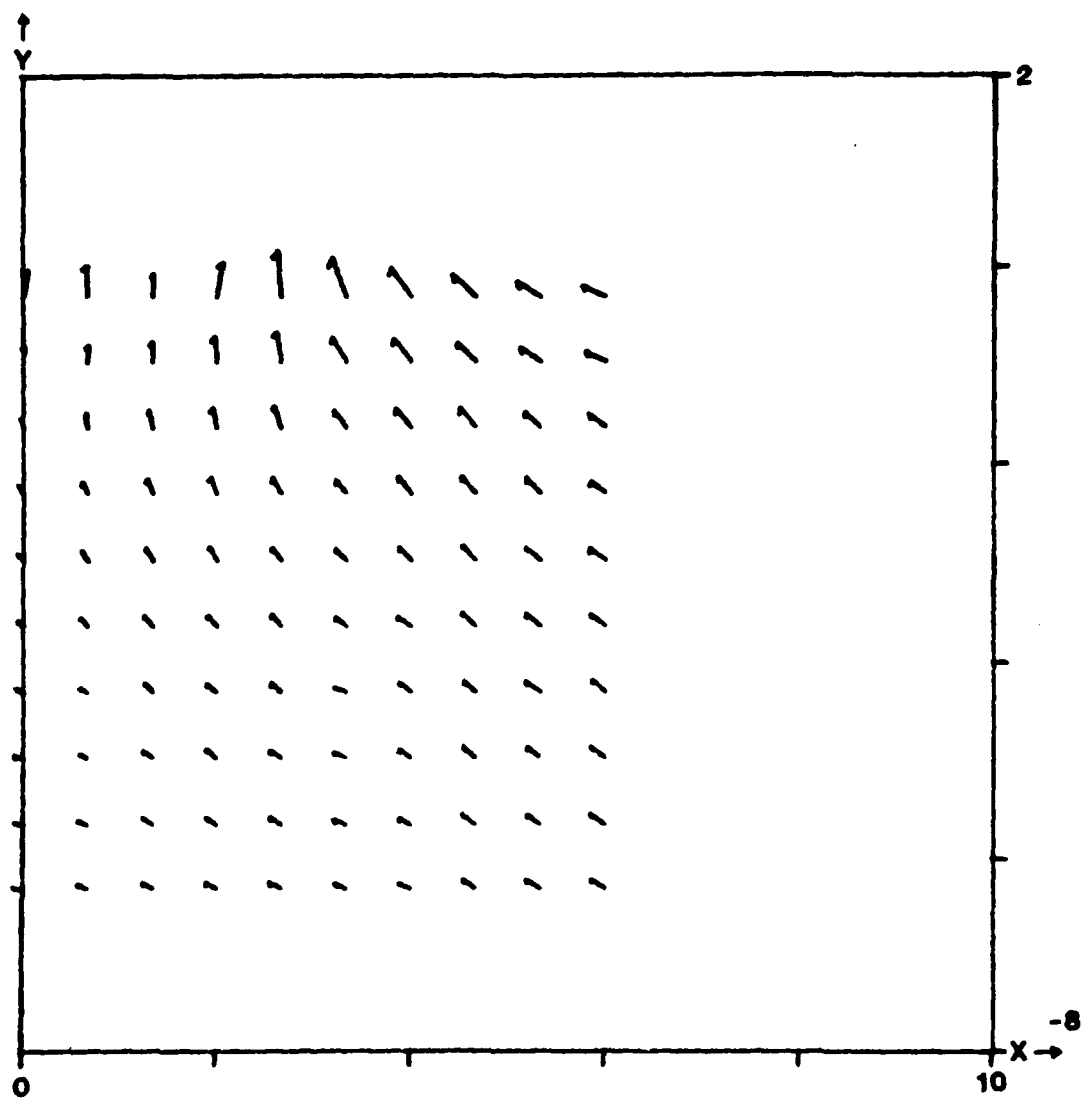
Figure B4. Cross Velocity Field for Streamwise Station -6

51
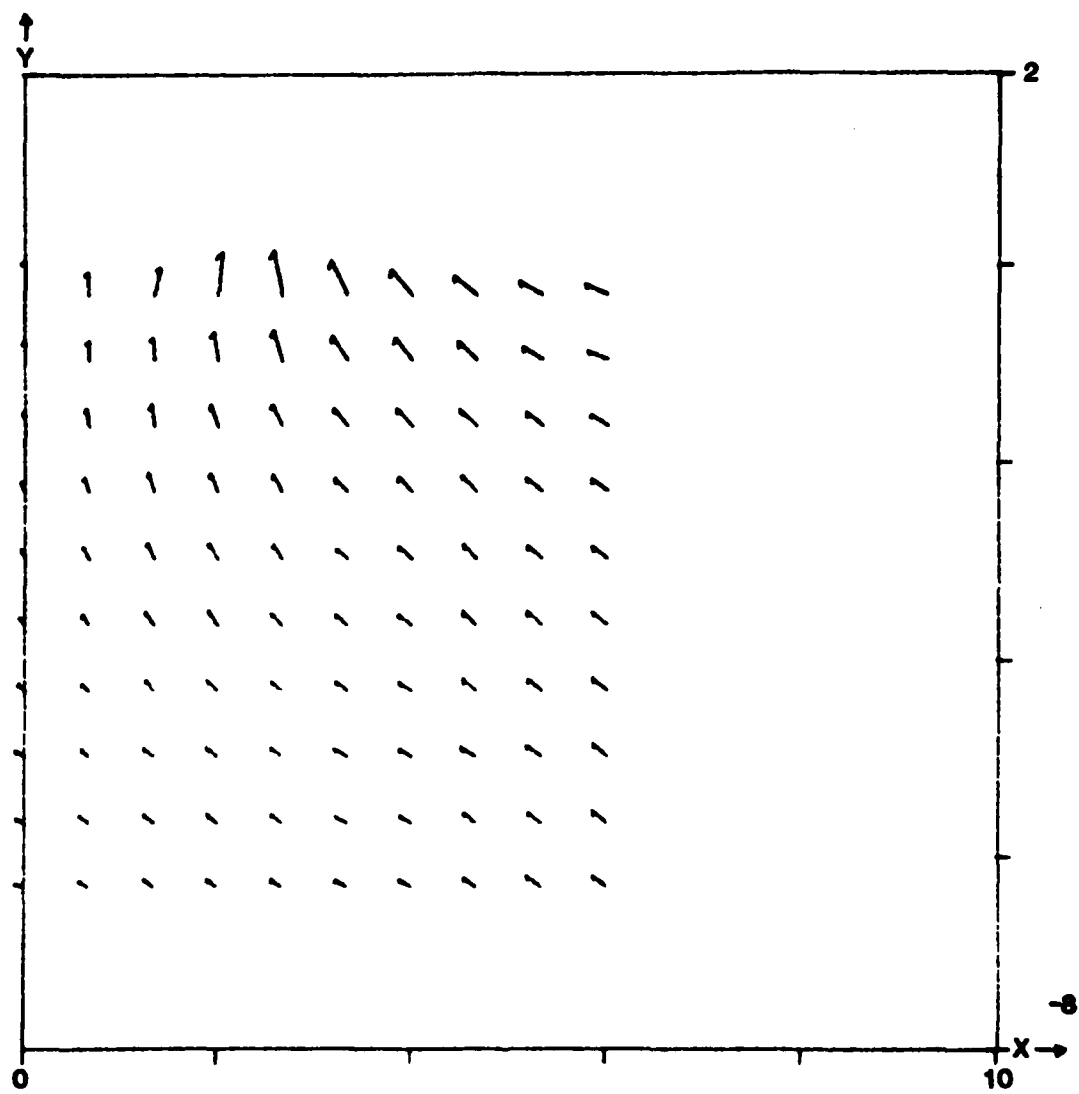
Figure B5. Cross Velocity Field for Streamwise Station -8

52
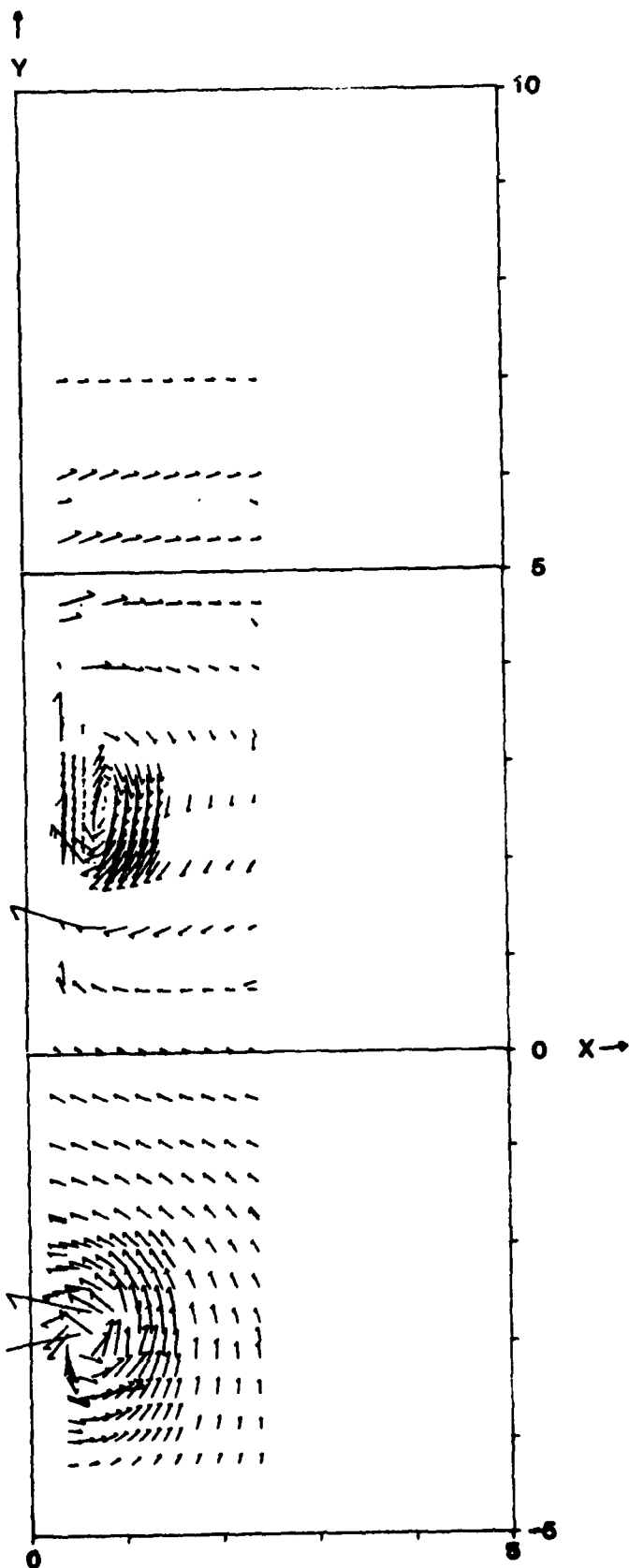
Figure WB1. Cross Velocity Vectors in the x-y Plane for Wing/
Body at Streamwise Station 0
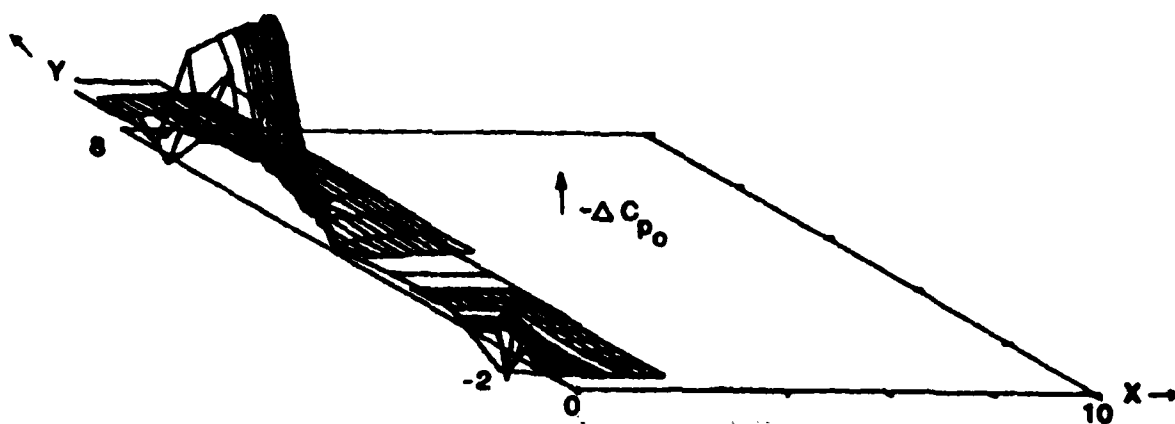
53

Figure WB2. ΔC_{p_o} Axonometric Plot for Wing/Body Configuration at Steamwise Station 0

Figure WB3. ΔC_{p_o} Axonometric Plot for Wing/Body Configuration at Streamwise Station 0

54

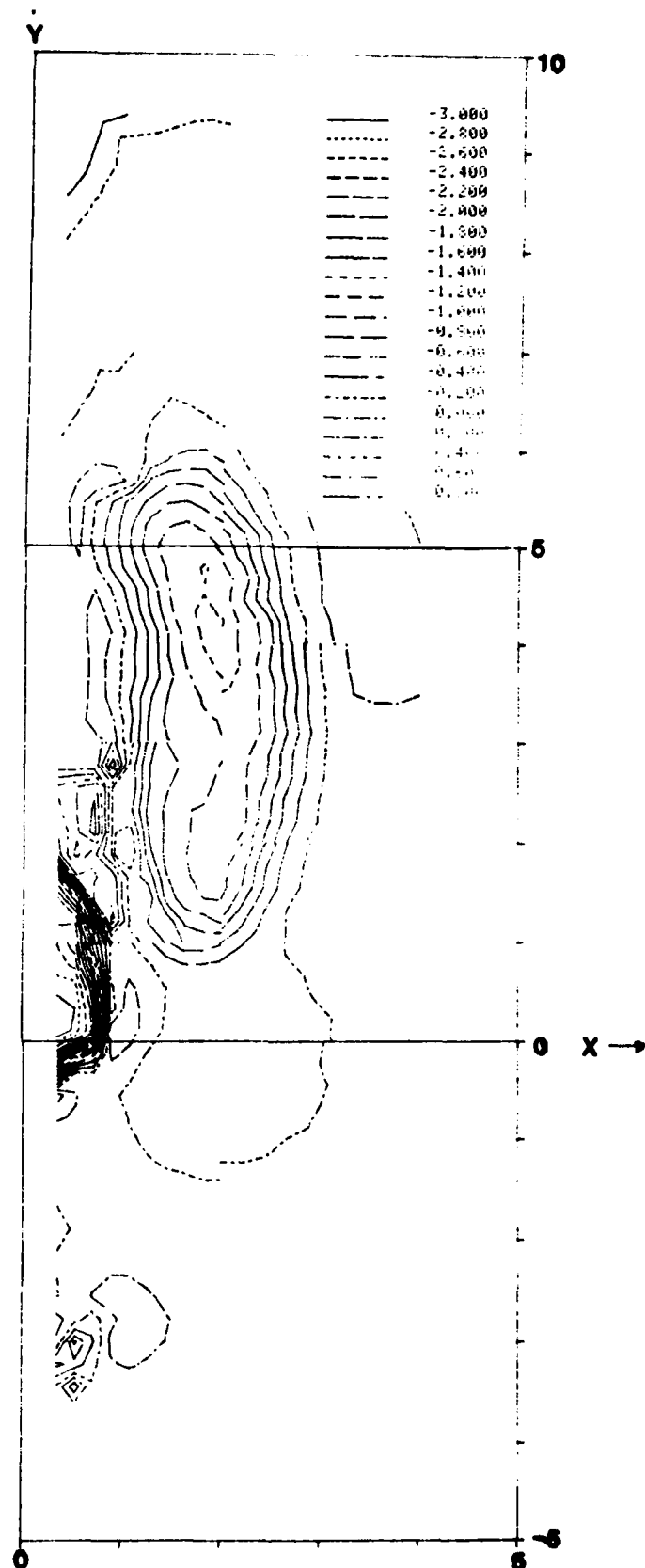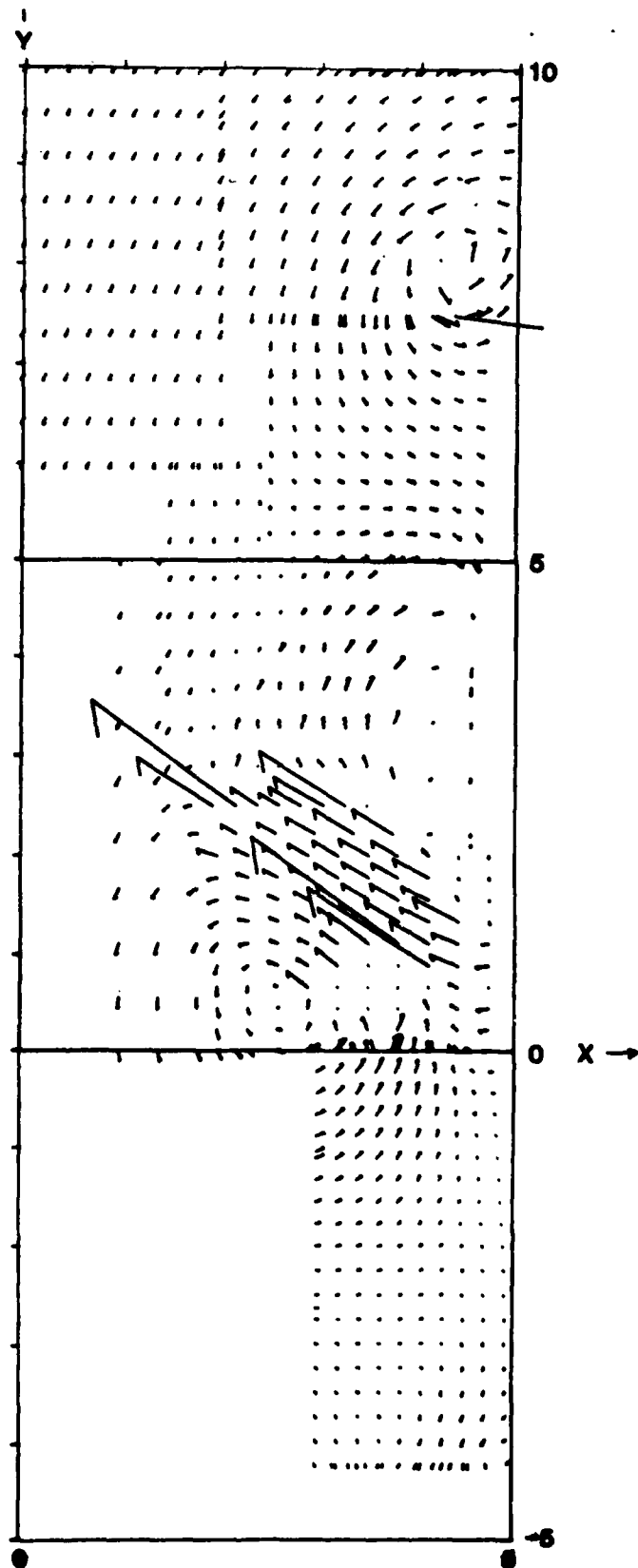Figure WB4. ΔC_{p_o} Axonometric Plot for Wing/Body Configuration at Streamwise Station 0

55
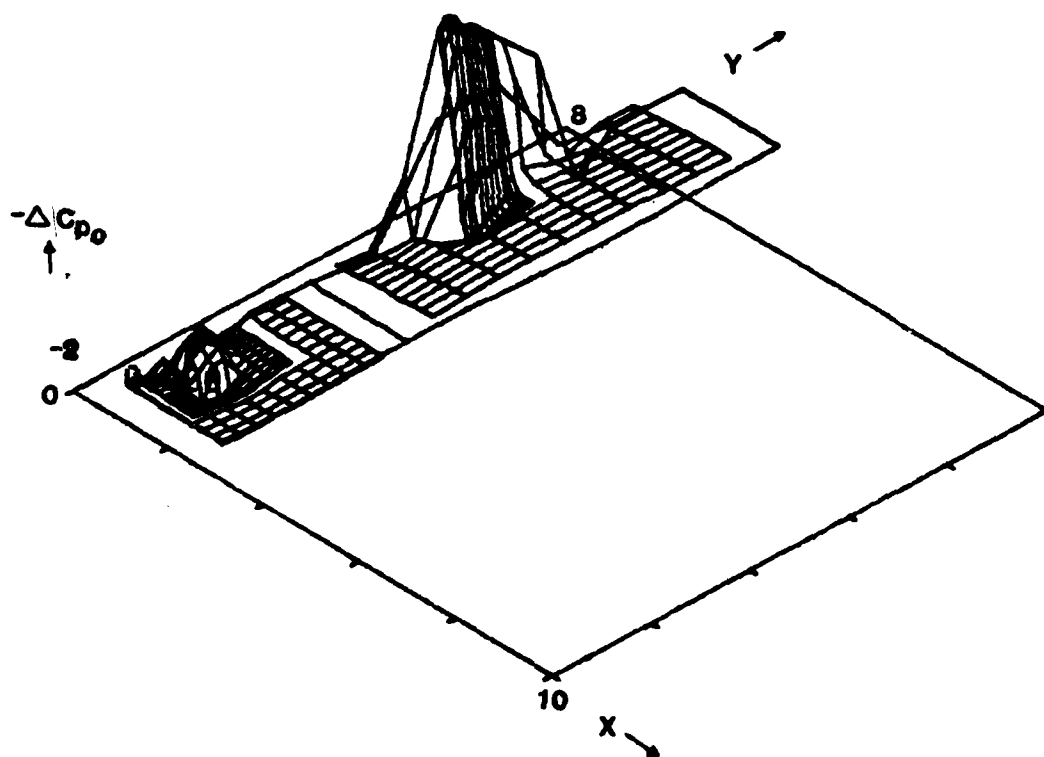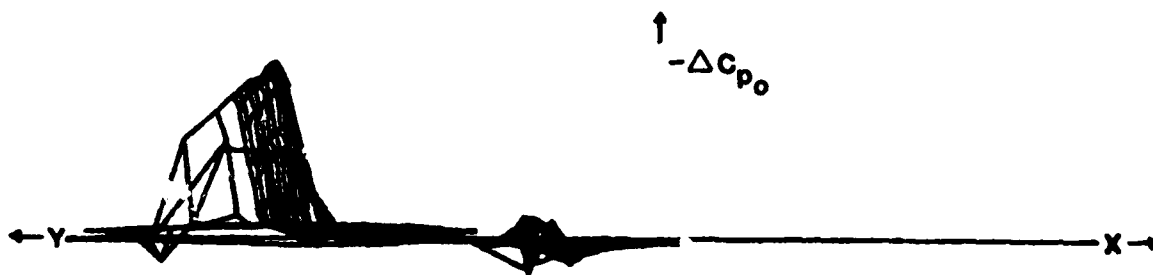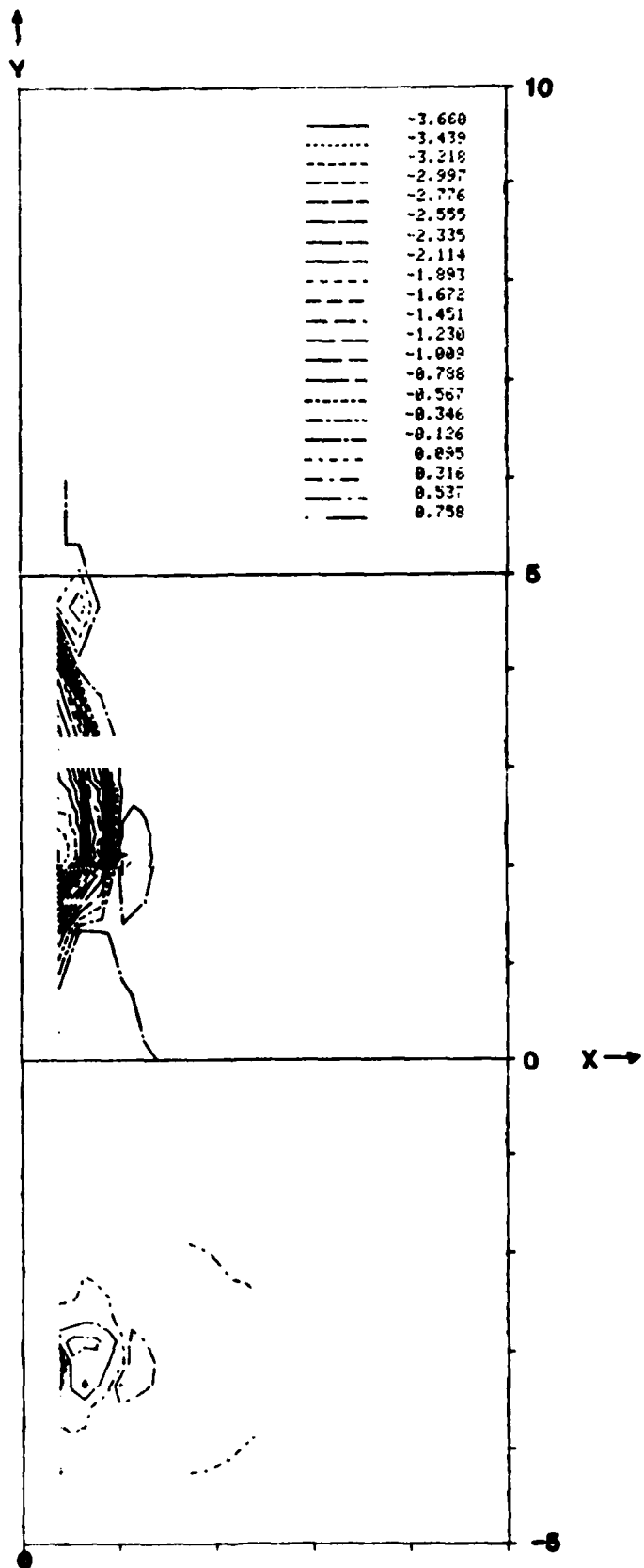
Figure WB5. Contour Plots of ΔC_{Po} in the x-y Plane for Wing/
Body at Streamwise Station 0
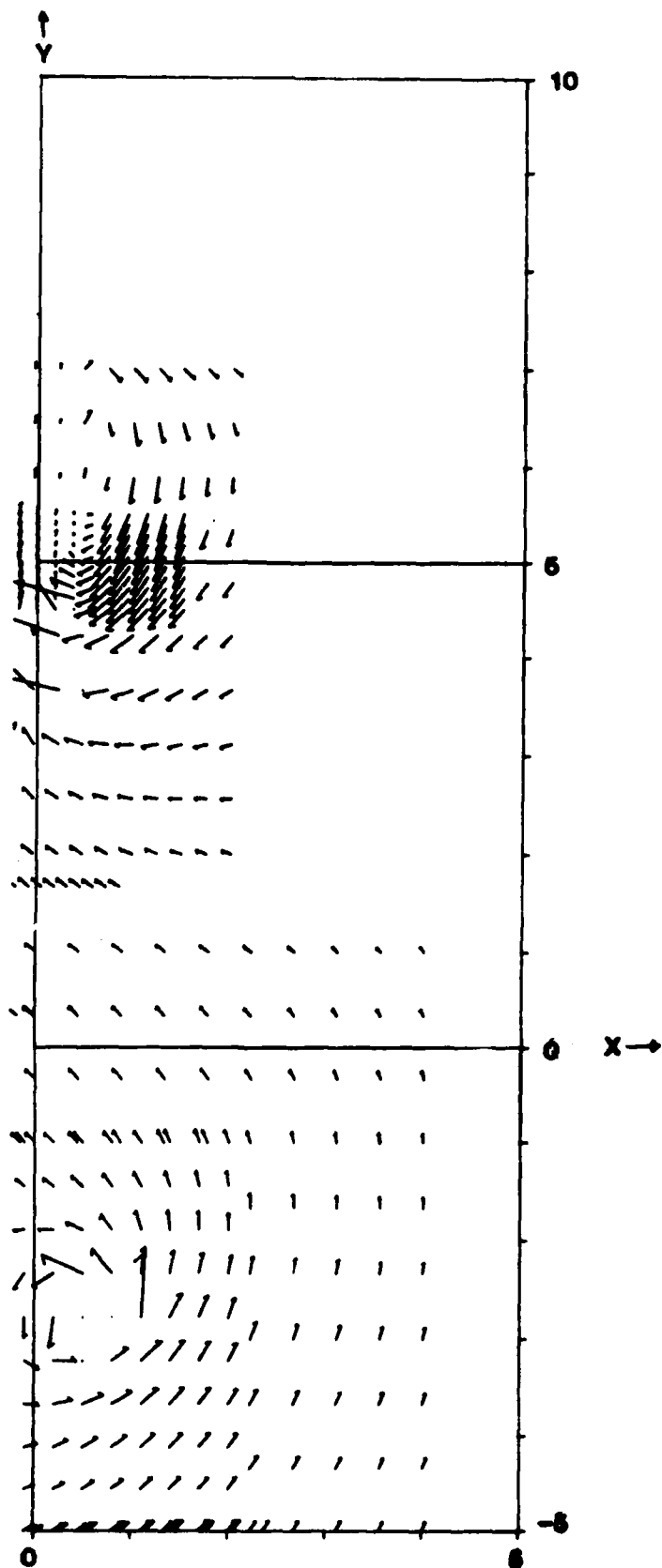
Figure WB6.   Cross Velocity Vectors in the x-y Plane for Wing/
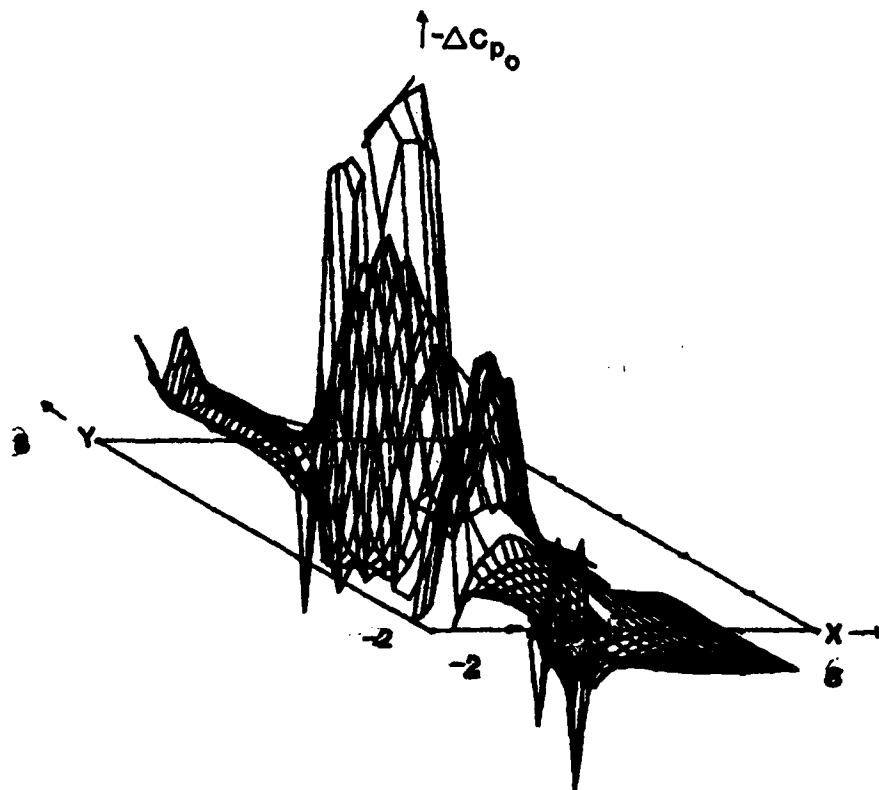Body at Streamwise Station -4
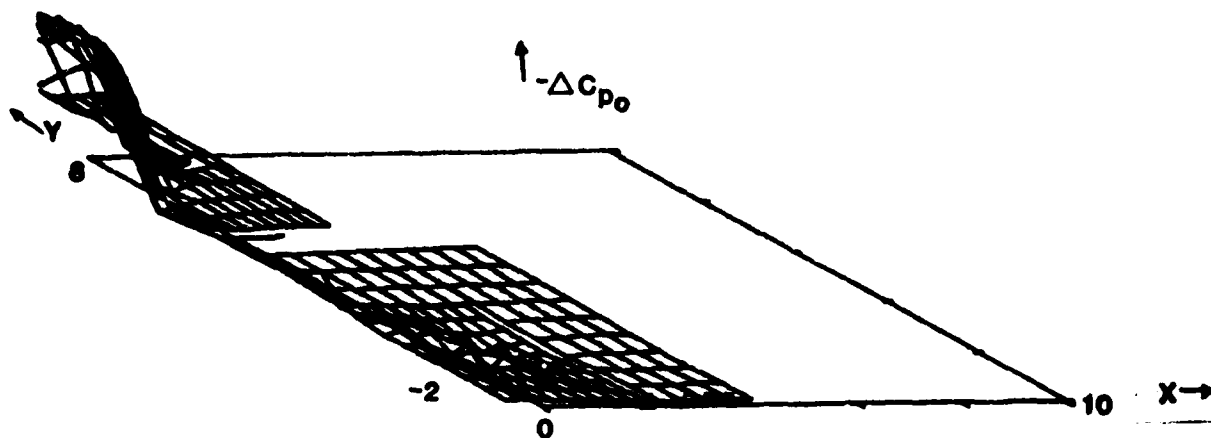
57

Figure WB7. ΔC_{p_o} Axonometric Plot for Wing/Body Configuration
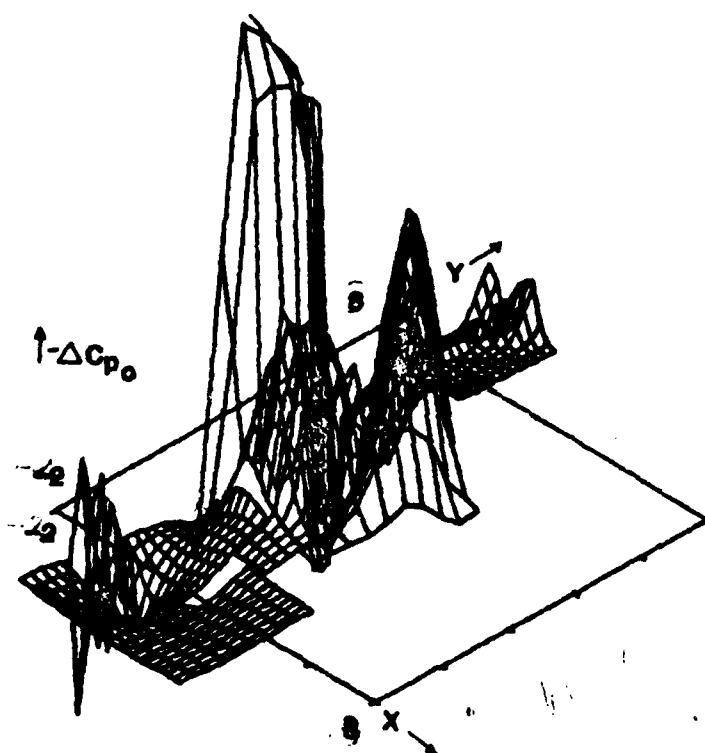at Streamwise Station -4

Figure WB8. ΔC_{p_o} Axonometric Plot for Wing/Body Configuration
at Streamwise Station -4
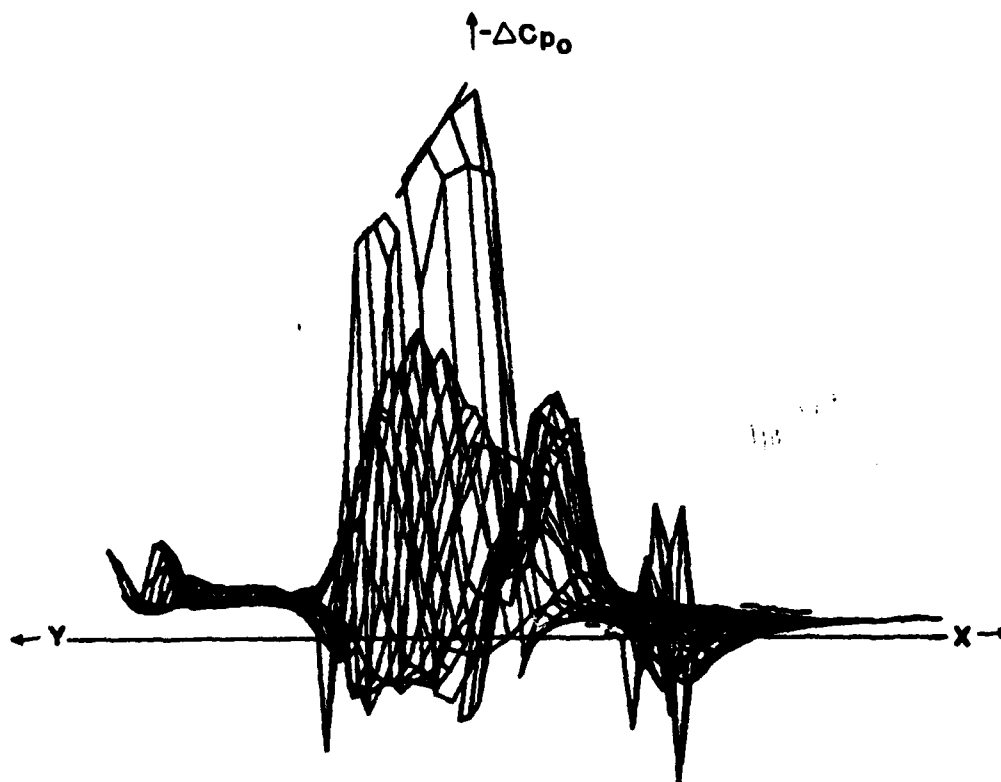
58
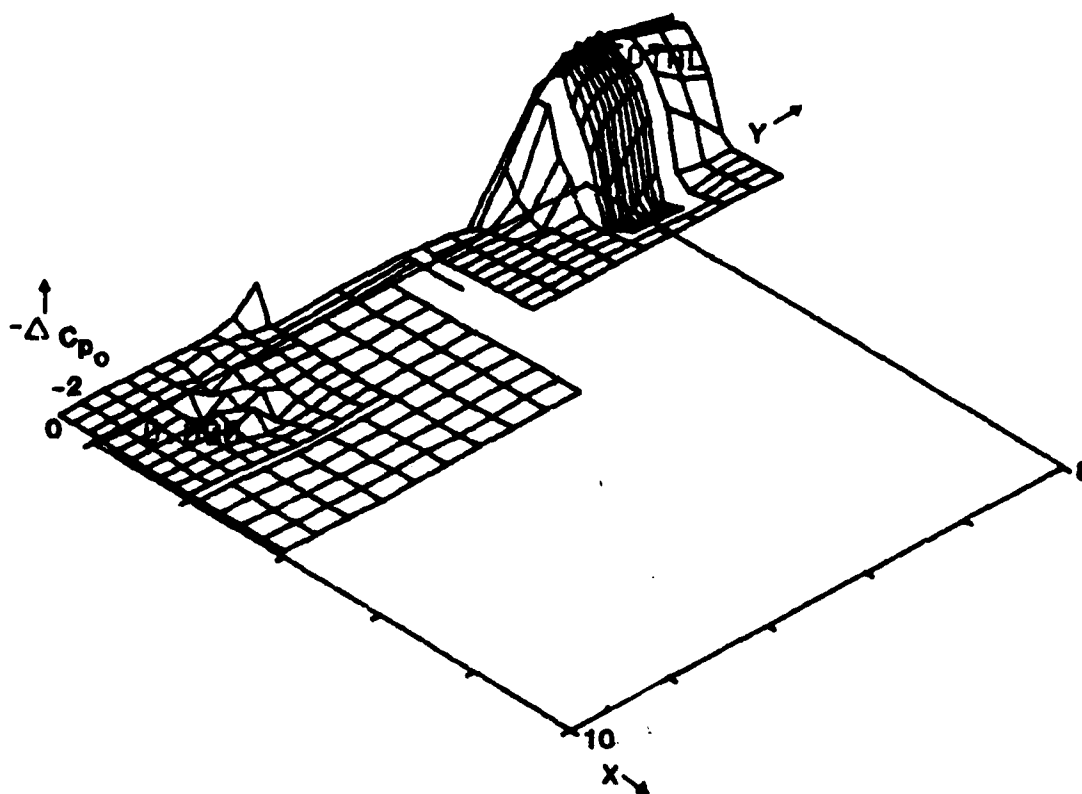
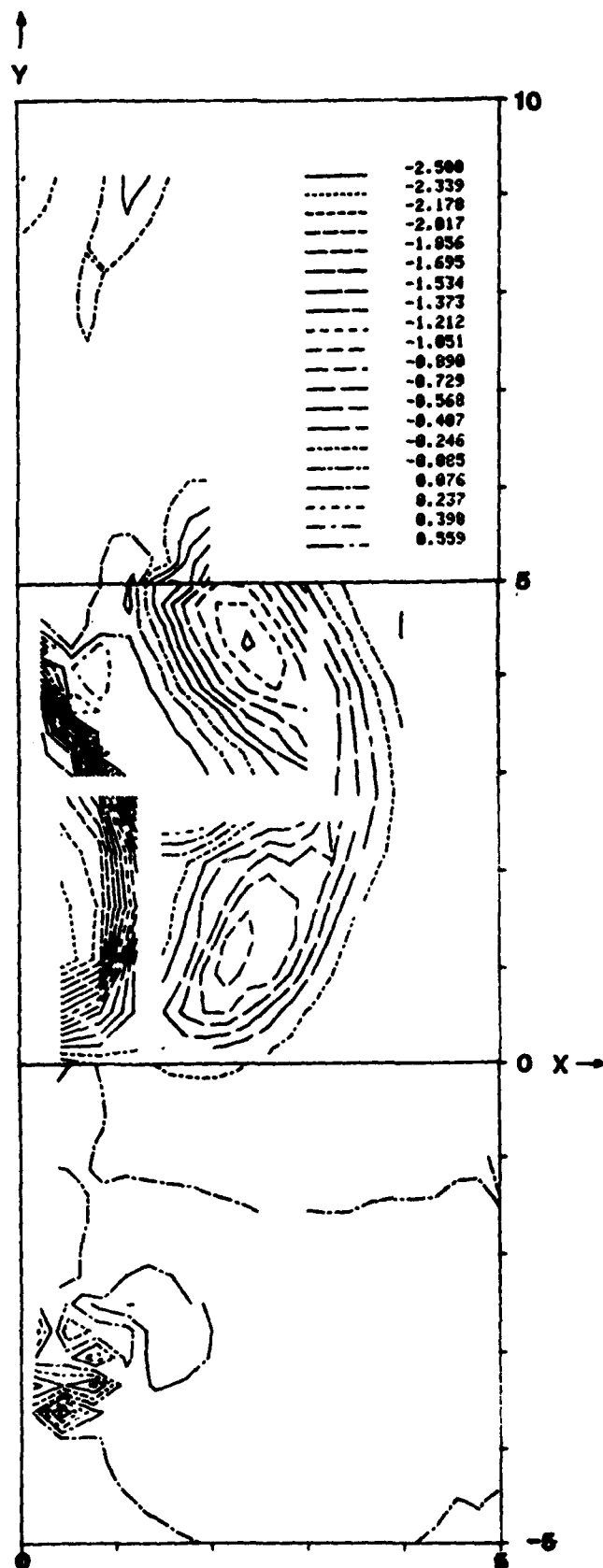Figure WB9. ΔC_{p_O} Axonometric Plot for Wing/Body Configuration at Streamwise Station -4
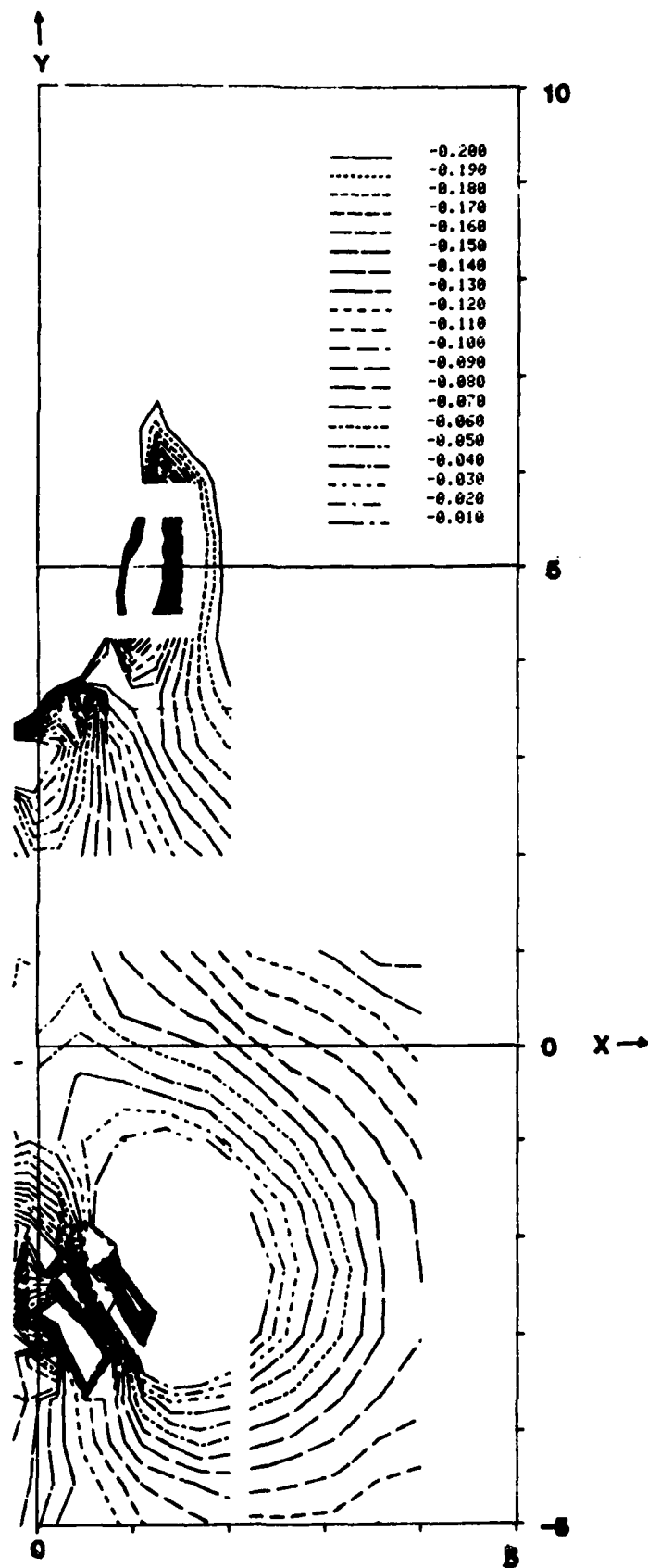
Figure WB10. Contour Plots of ΔC_{Po} in the x-y Plane for Wing/ Body at Streamwise Station -4
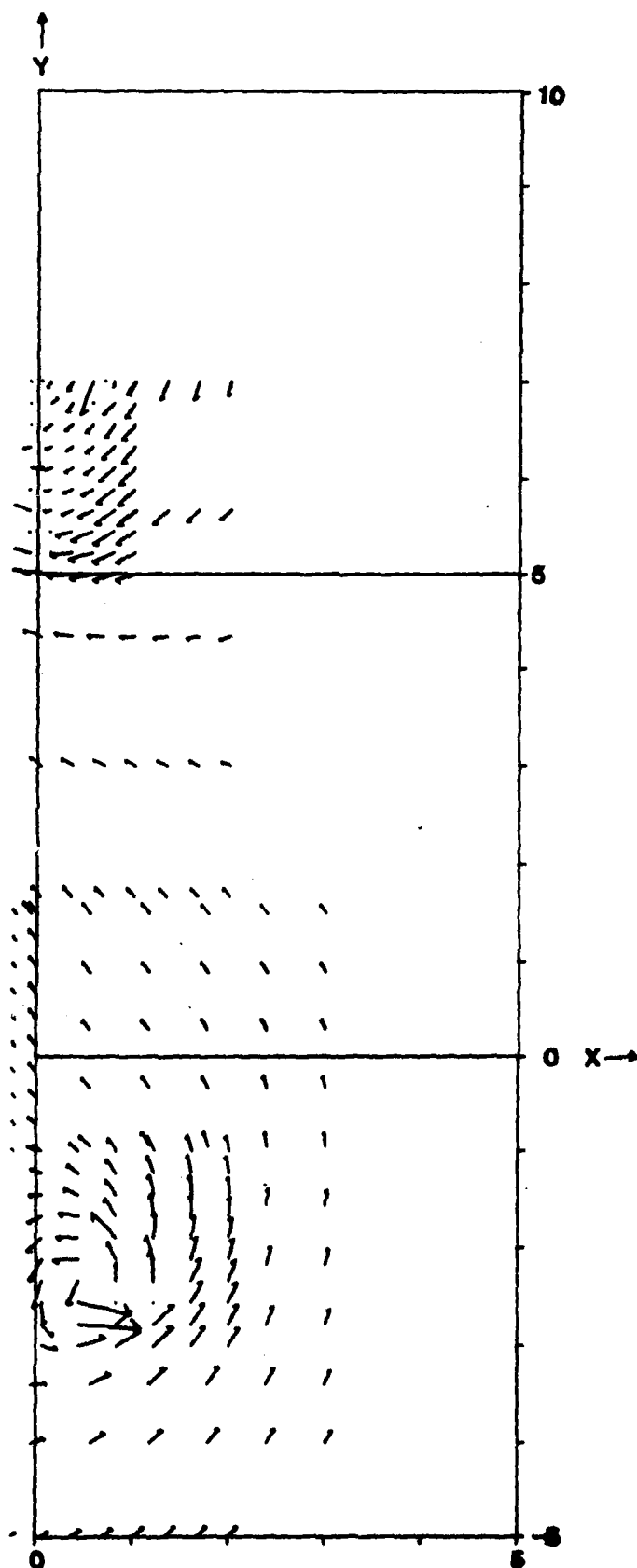
Figure WB11. Cross Velocity Vectors in the x-y Plane for Wing/
Body at Streamwise Station -8
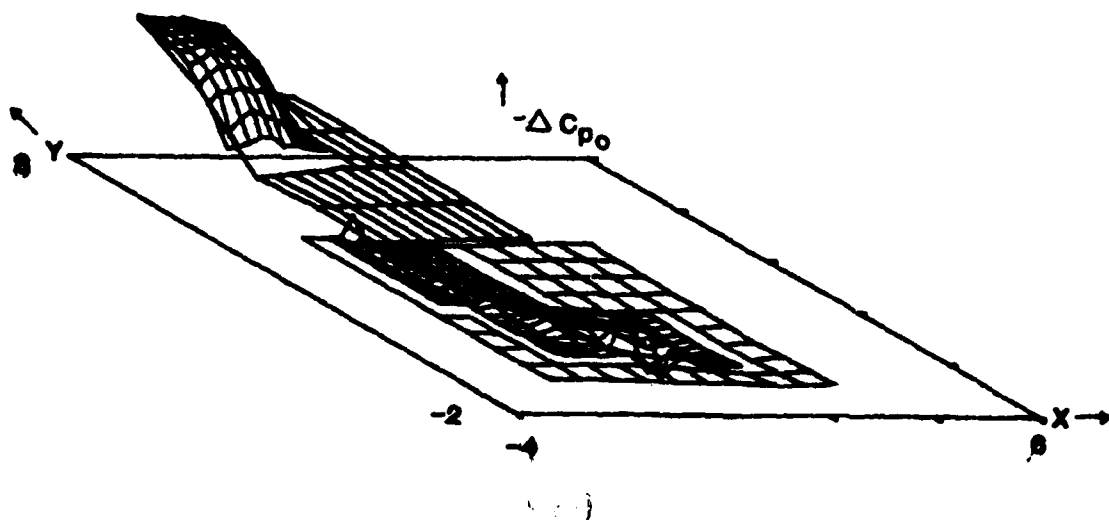
61

Figure WB12. ΔC_{po} Axonometric Plot for Wing/Body Configuration at Streamwise Station -8
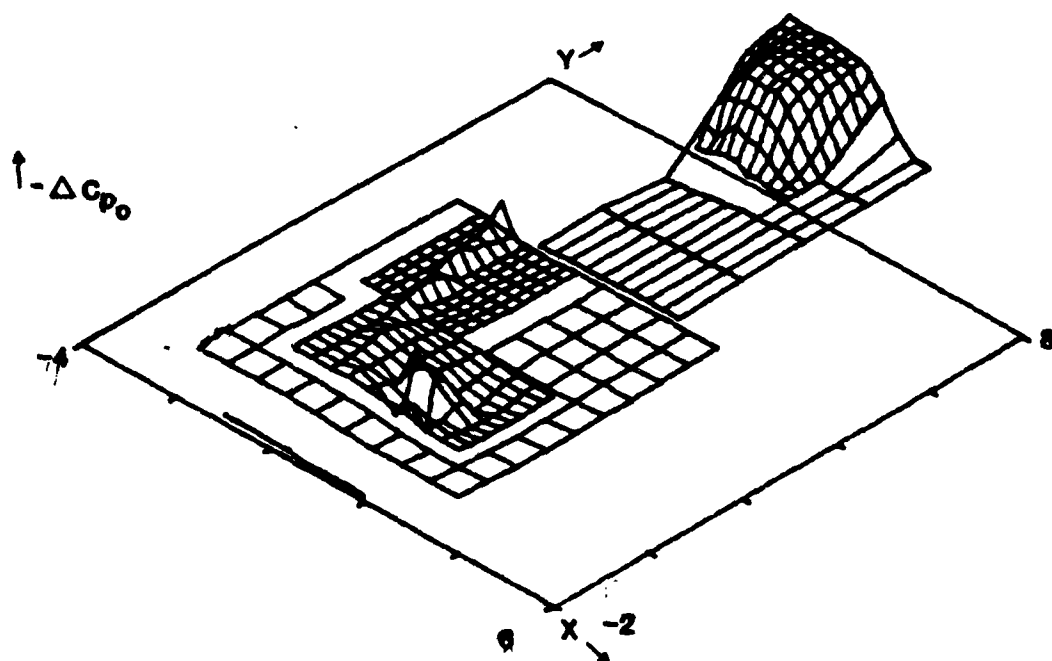
Figure WB13. ΔC_{po} Axonometric Plot for Wing/Body Configuration at Streamwise Station -8
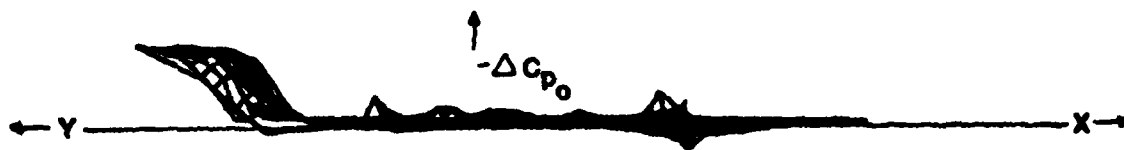
Figure WB14. ΔC_{Po} Axonometric Plot for Wing/Body Configuration
at Streamwise Station -8
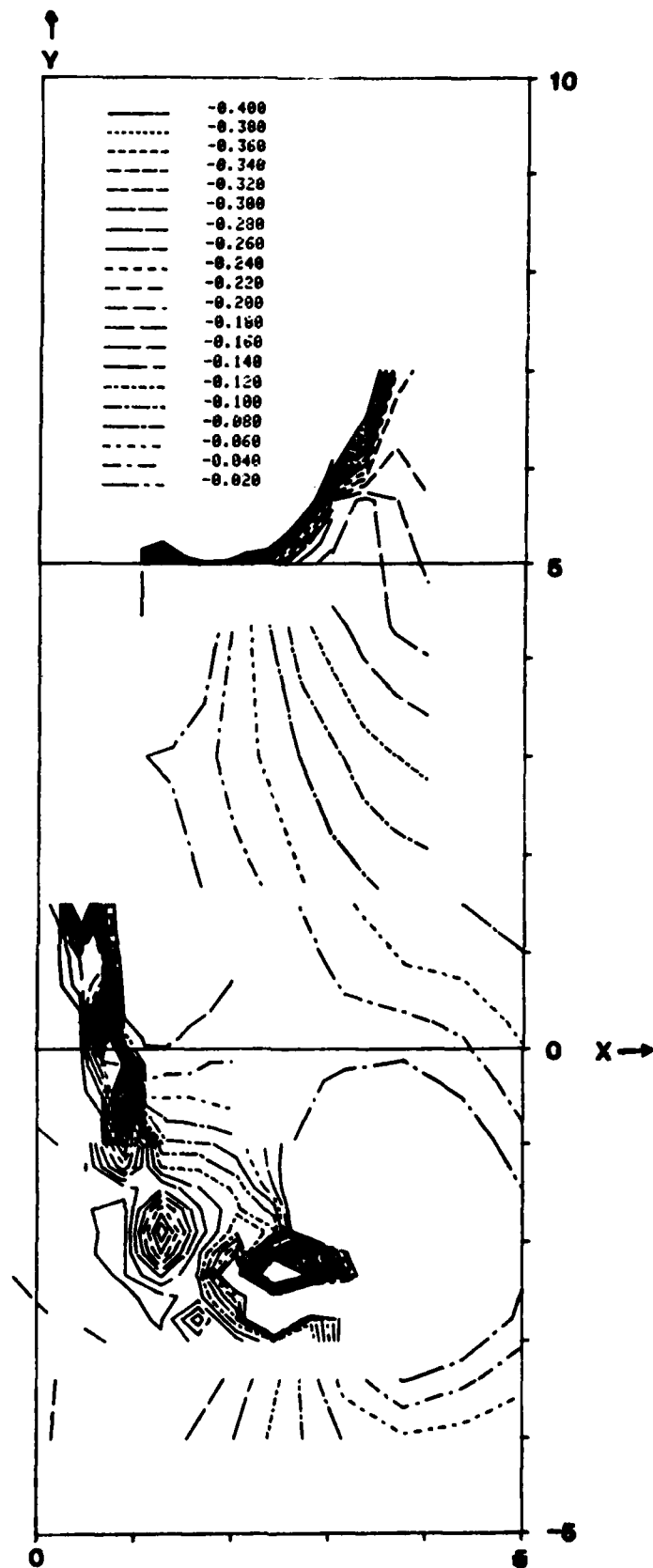
Figure WB15. Contour Plots of ΔC_{Po} in the x-y Plane for Wing/Body at Streamwise Station-18
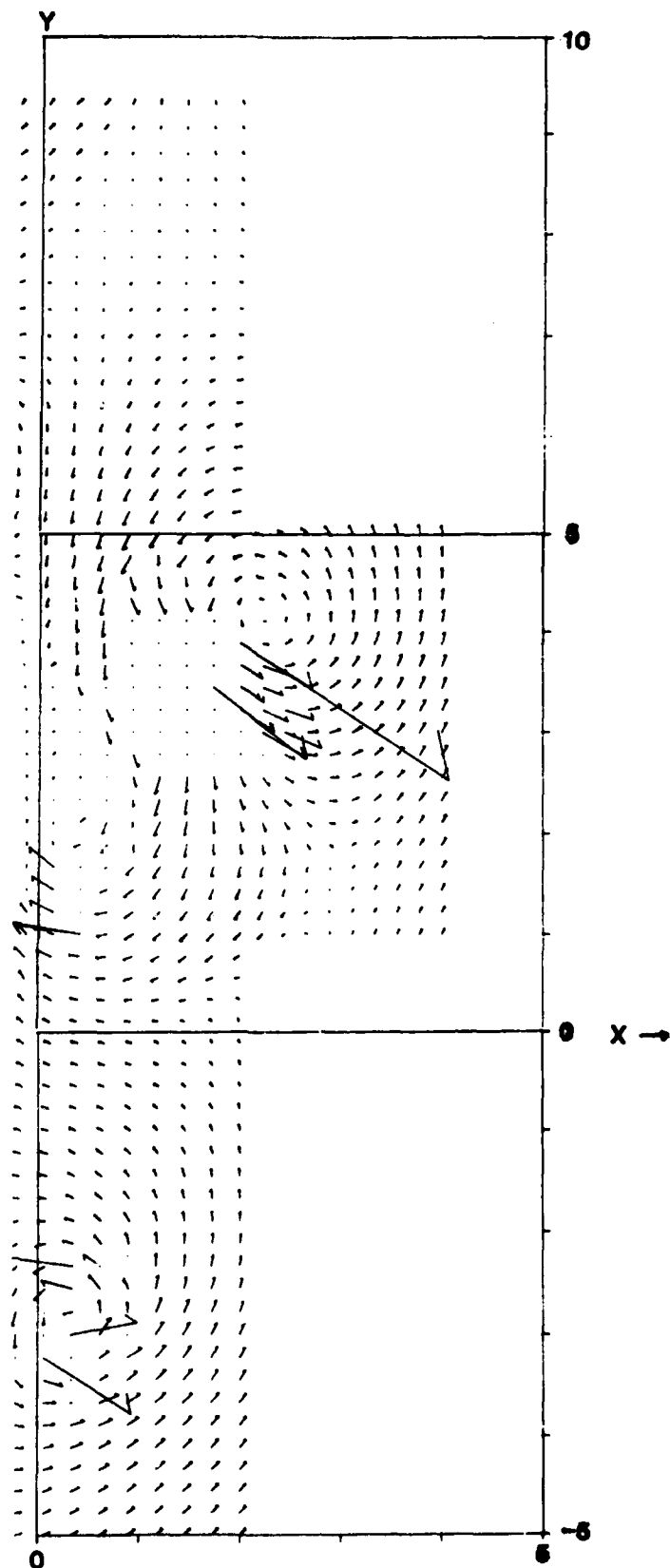
64
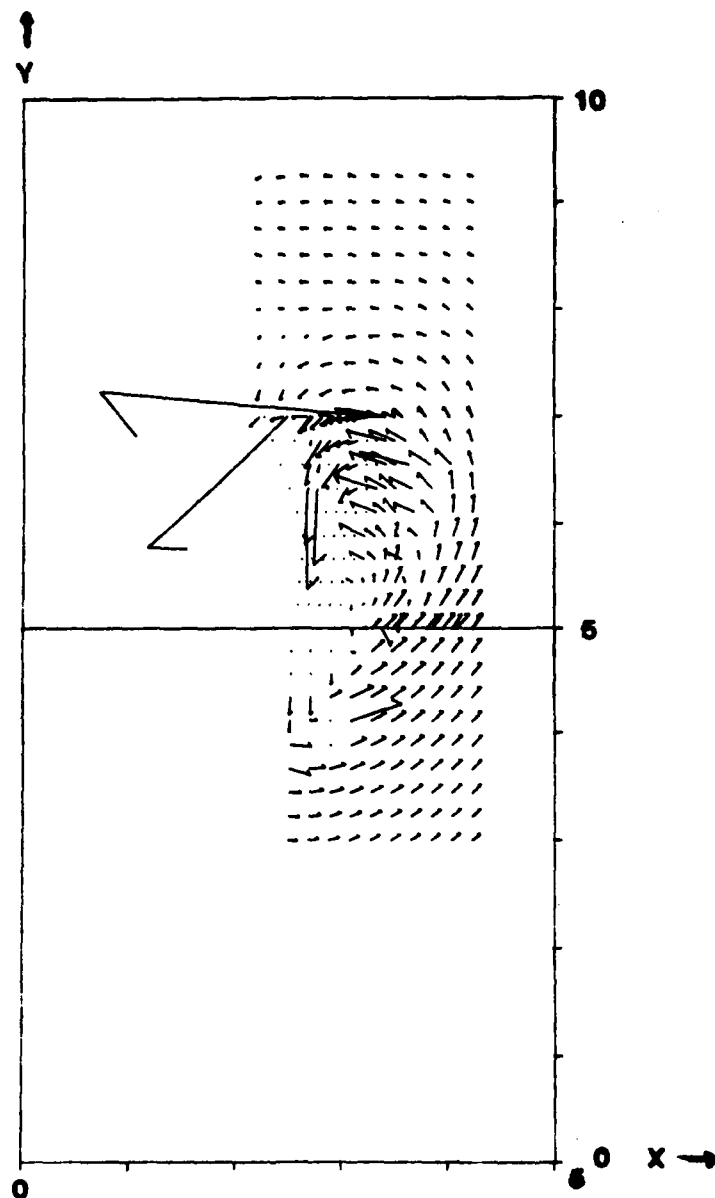
Figure WBC1. Cross Velocity Vectors in the x-y Plane for Wing/
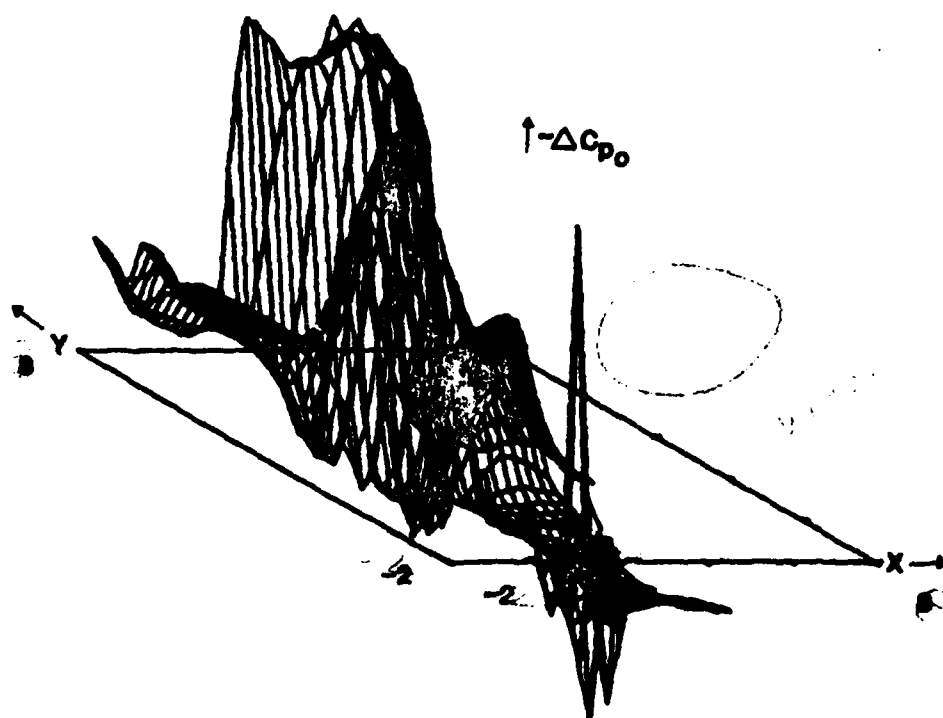Body/Canard at Streamwise Station 9:
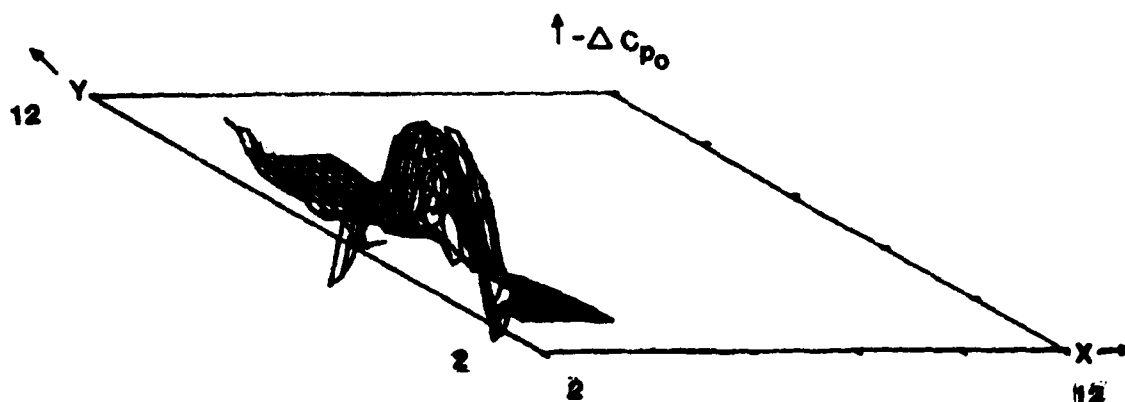
Figure WBC2.　ΔC_{Po}　Axonometric Plot for Wing/Body/Canard
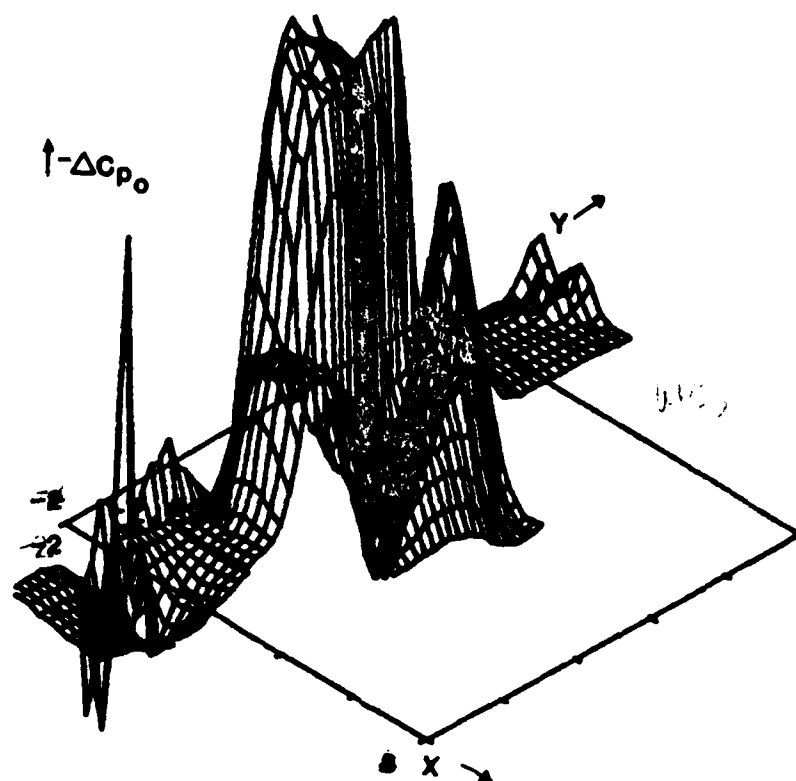Configuration at Streamwise Station 9
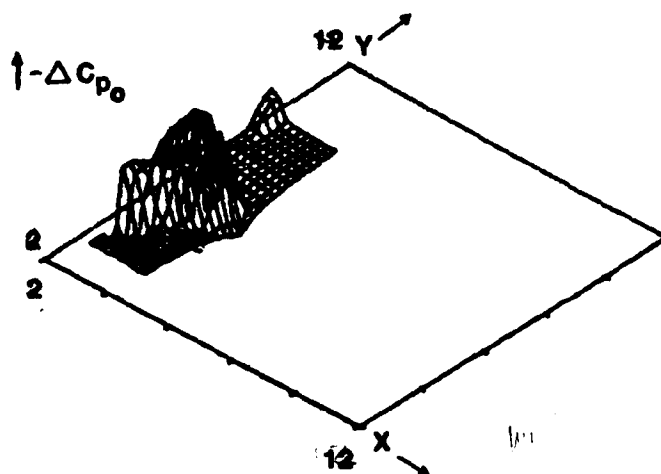
Figure WBC3.　ΔC_{Po}　Axonometric Plot for Wing/Body/Canard
Configuration at Streamwise Station 9

Figure WBC4.　ΔC_{Po}　Axonometric Plot for Wing/Body/Canard
Configuration at Streamwise Station 9

66
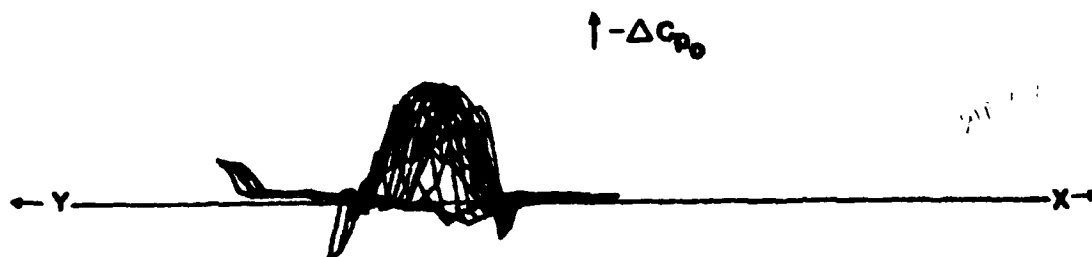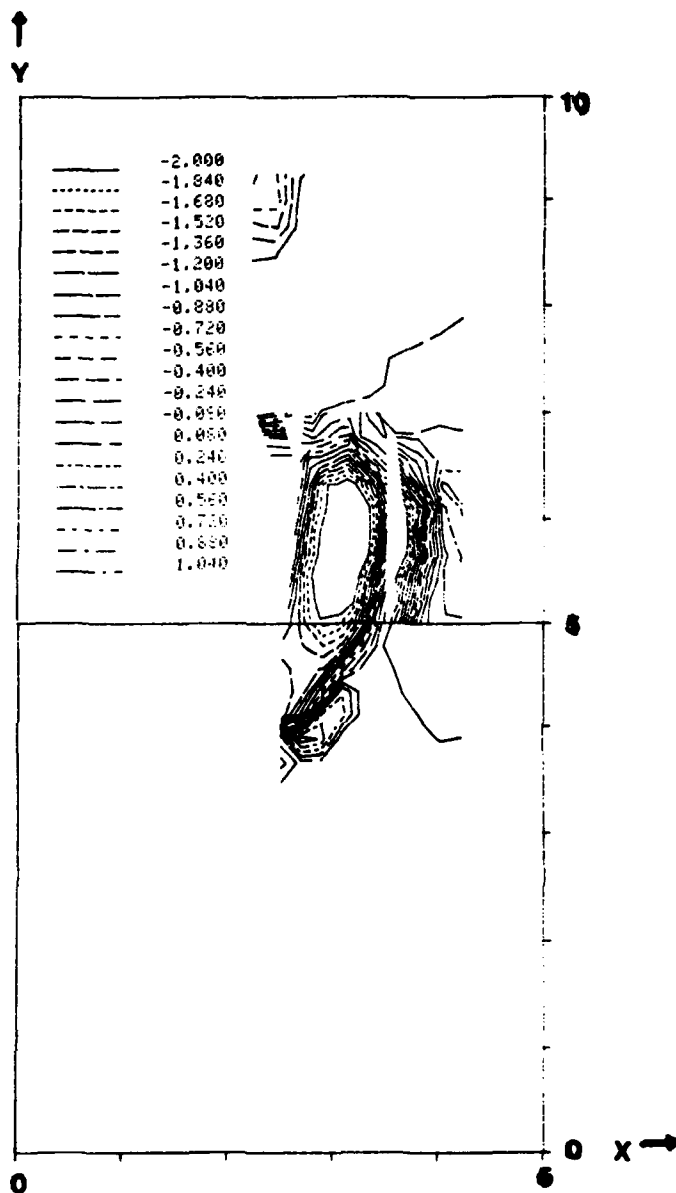
Figure WBC5. Contour Plots of ΔC_{Po} in the x-y Plane for Wing/
Body/Canard at Streamwise Station 9

67
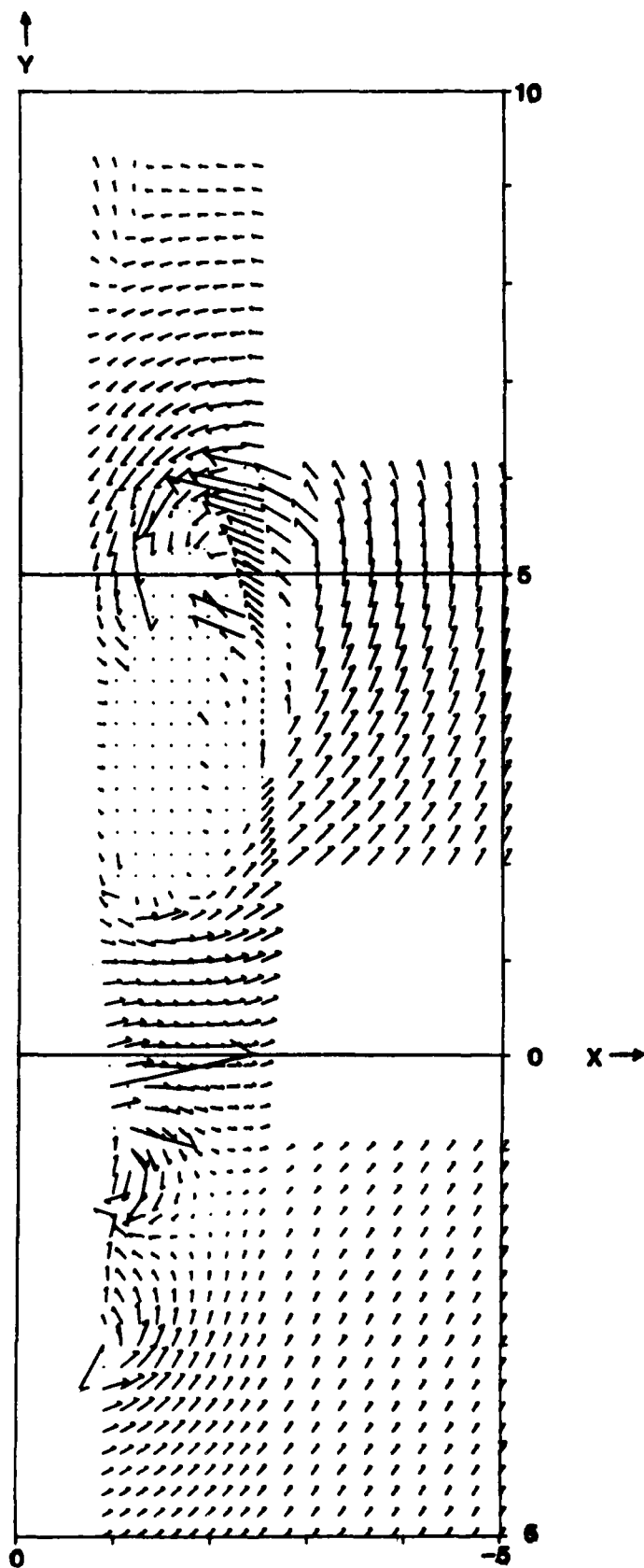
Figure WBC6.   Cross Velocity Vectors in the x-y Plane for Wing/
                Body/Canard at Streamwise Station 4;
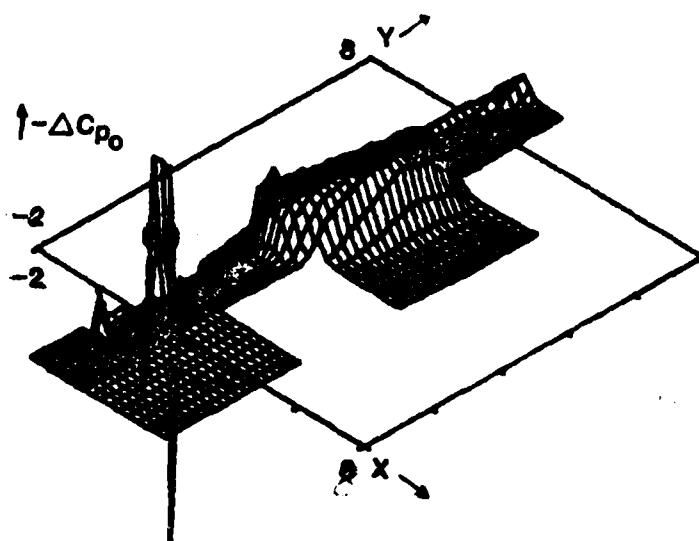
68

Figure WBC7.　ΔC_{Po}　Axonometric Plot for Wing/Body/Canard
Configuration at Streamwise Station 4

Figure WBC8.　ΔC_{Po}　Axonometric Plot for Wing/Body/Canard
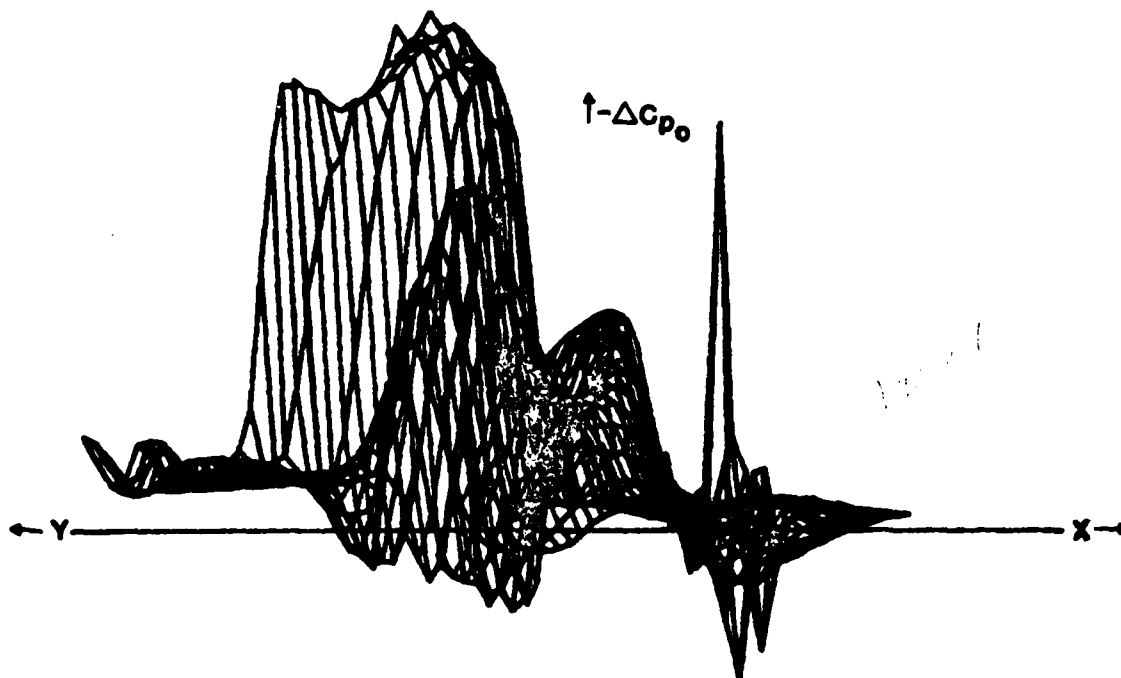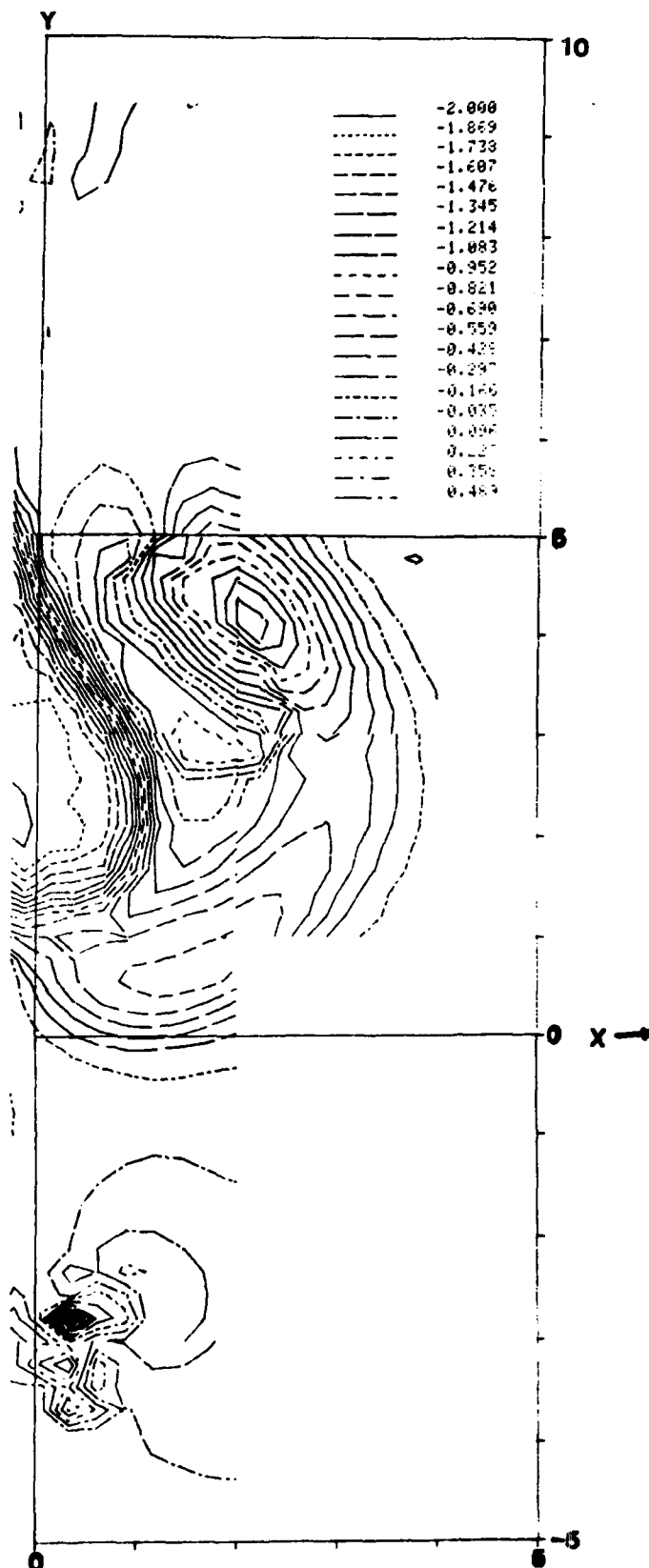Configuration at Streamwise Station 4

69
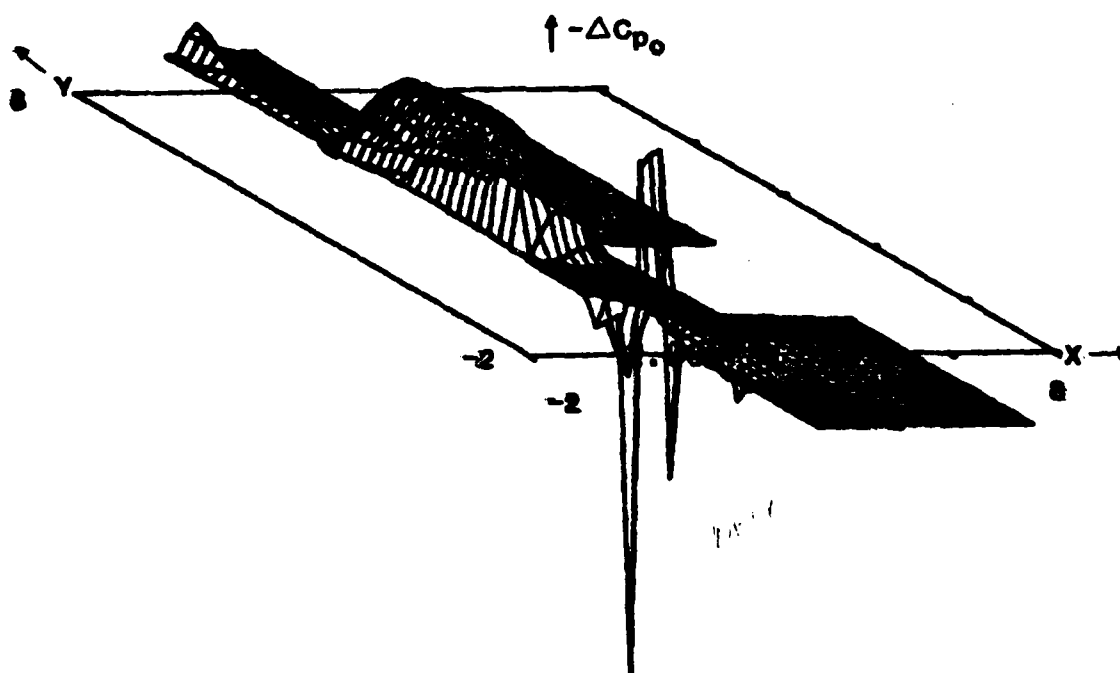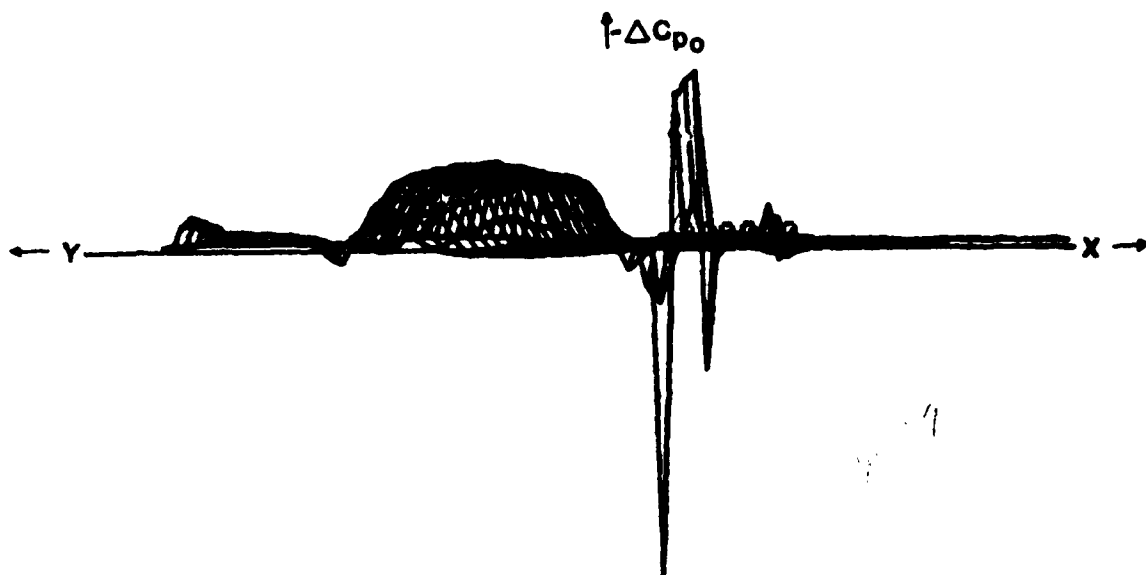
Figure WBC9. ΔC_{Po} Axonometric Plot for Wing/Body/Canard
Configuration at Streamwise Station 4
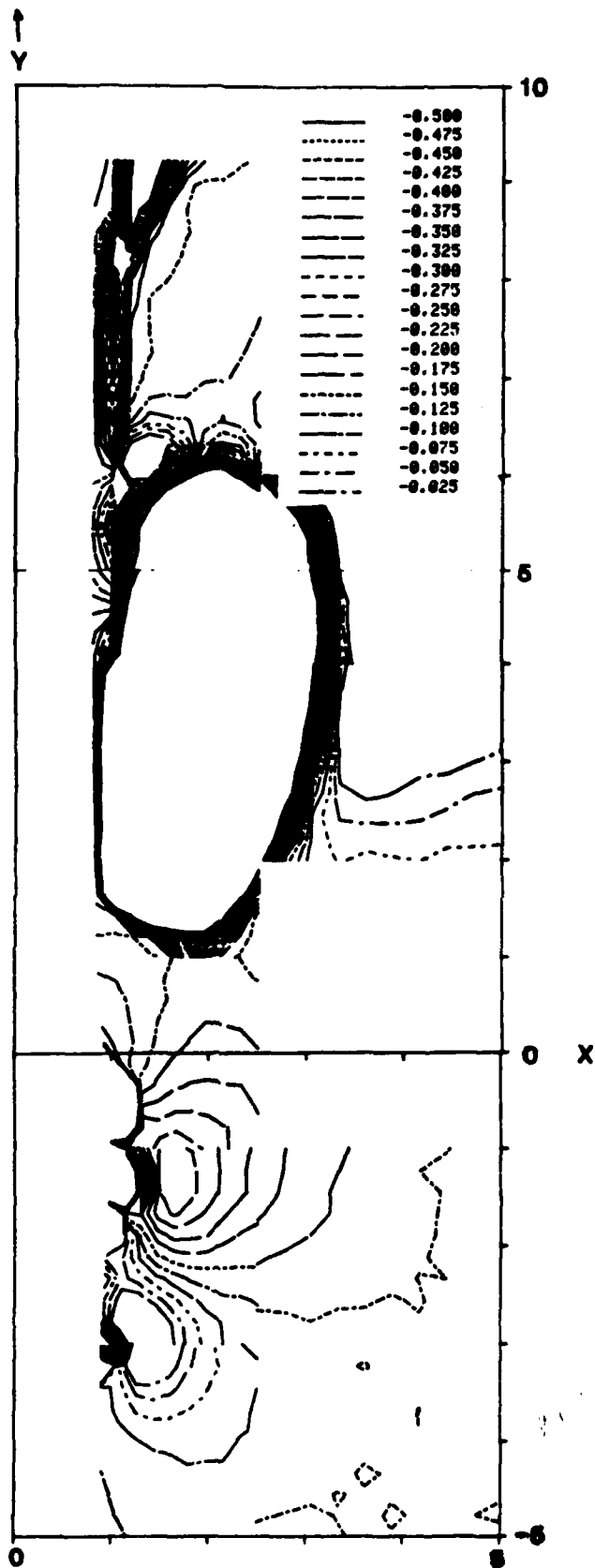
Figure WBC10. Contour Plots of ΔC_{Po} in the x-y Plane for Wing/
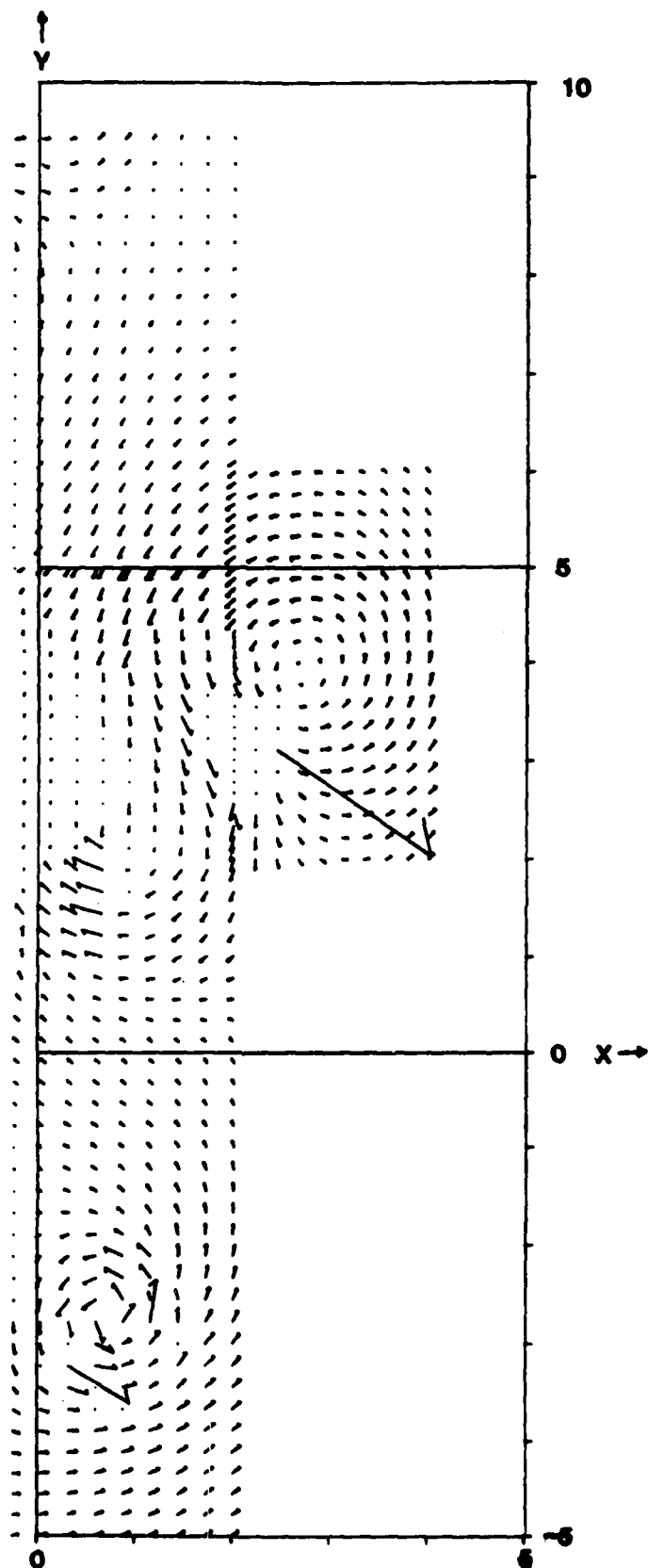Body/Canard at Streamwise Station 4

71
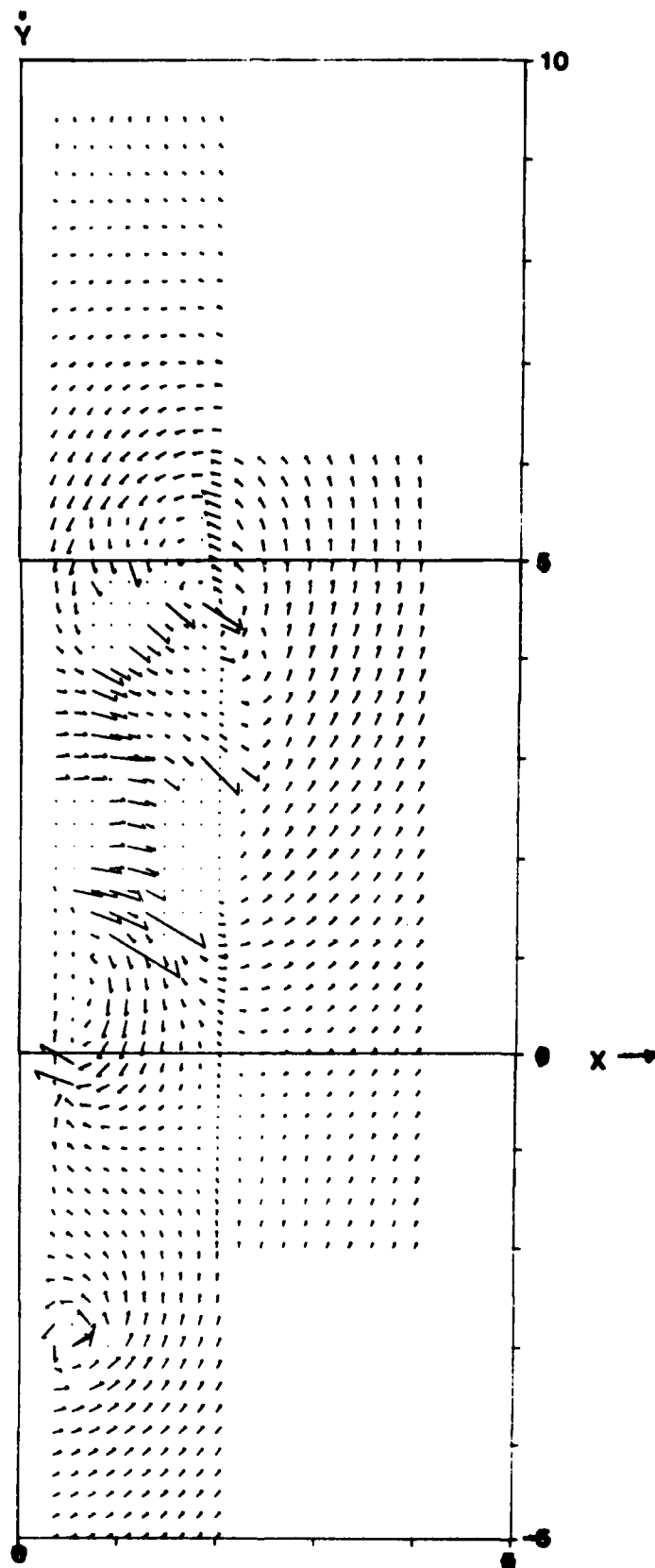
Figure WBC11. Cross Velocity Vectors in the x-y Plane for Wing/
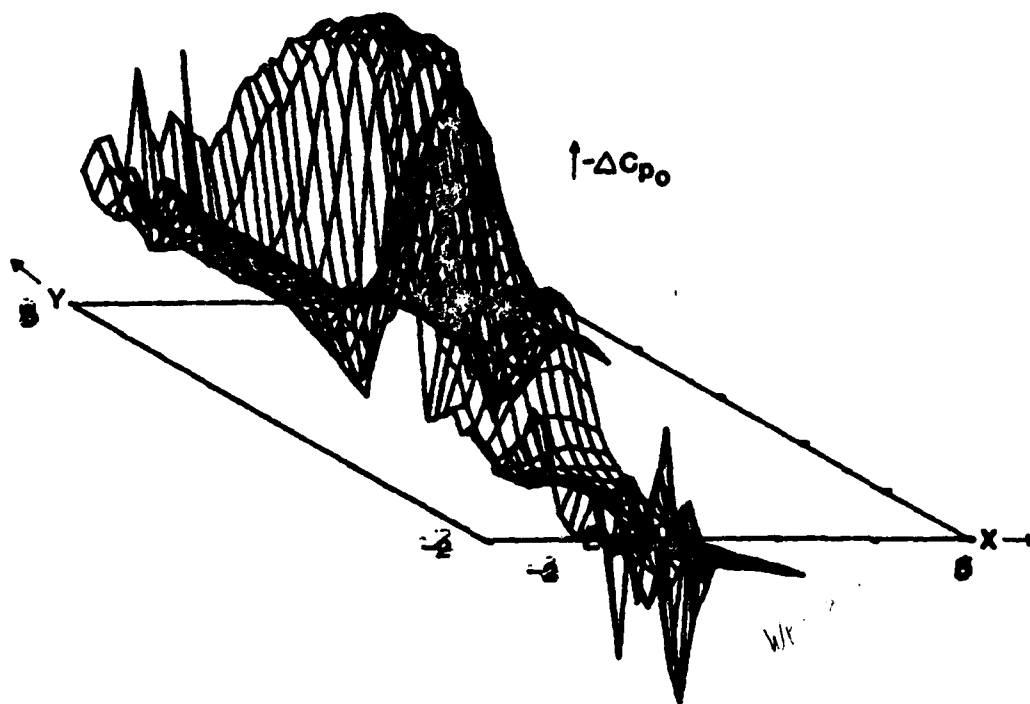Body/Canard at Streamwise Station 2.
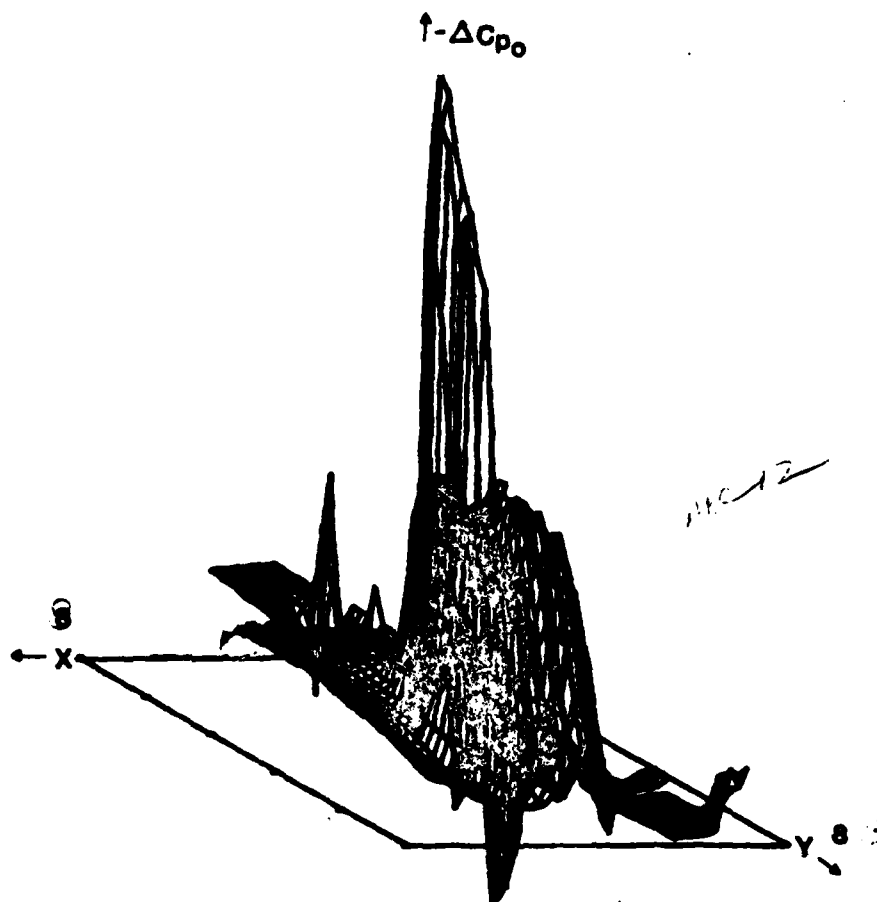
72

Figure WBC12. ΔC_{Po} Axonometric Plot for Wing/Body/Canard
Configuration at Streamwise Station 2
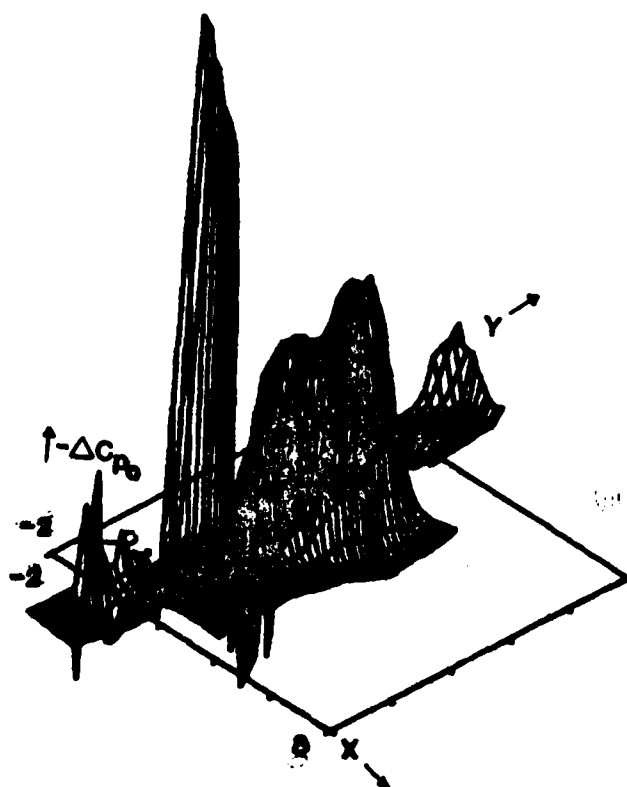
Figure WBC13. ΔC_{P_0} Axonometric Plot for Wing/Body/Canard
Configuration at Streamwise Station 2
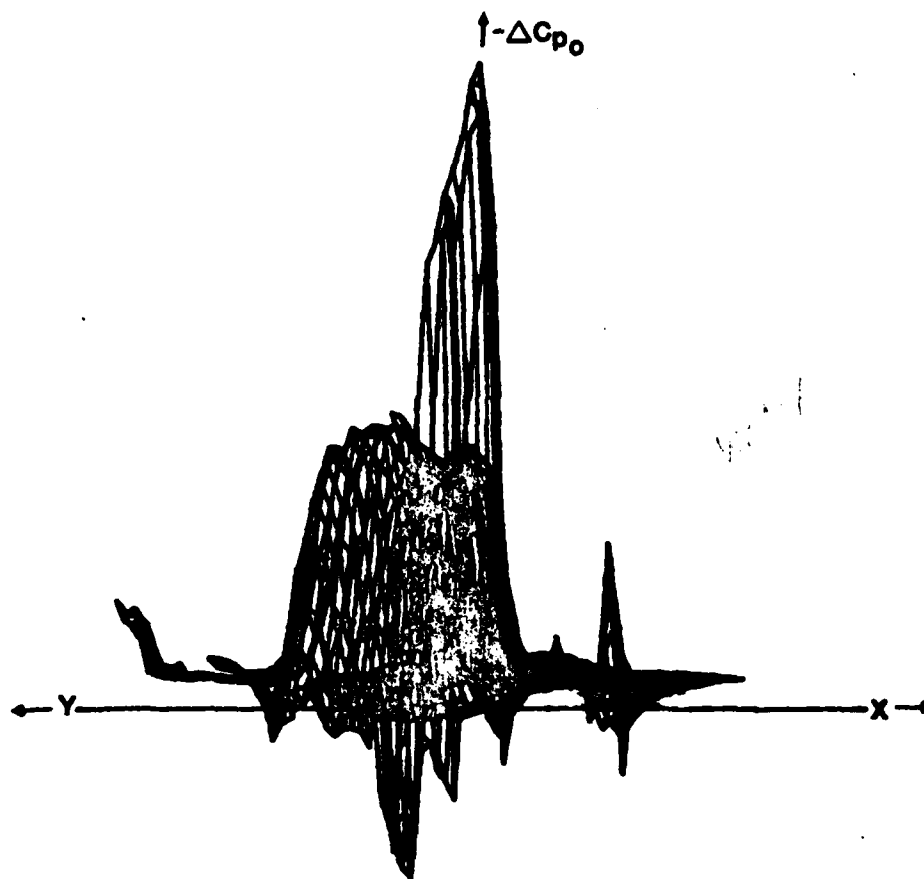
Figure WBC14. ΔC_{P_O} Axonometric Plot for Wing/Body/Canard
Configuration at Streamwise Station 2

Figure WBC15. Contour Plots of ΔC_{Po} in the x-y Plane for Wing/ Body/Canard at Streamwise Station 2.

Figure WBC16.   Cross Velocity Vectors in the x-y Plane for Wing/
Body/Canard at Streamwise Station 0

77

Figure WBC17. ΔC_{Po} Axonometric Plot for Wing/Body/Canard
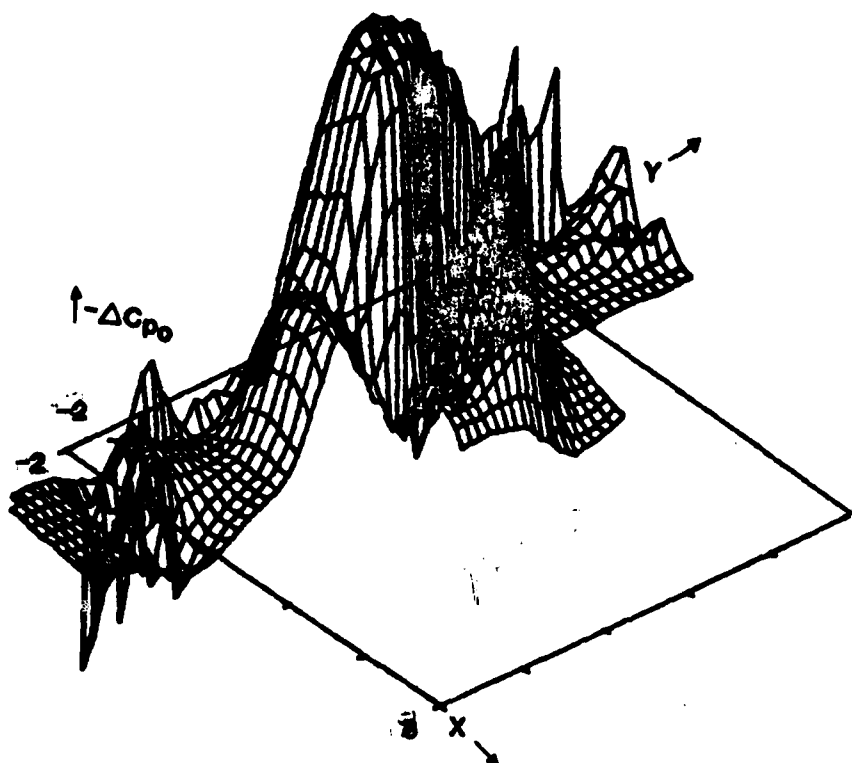Configuration at Streamwise Station 0

78

Figure WBC18. ΔC_{Po} Axonometric Plot for Wing/Body/Canard
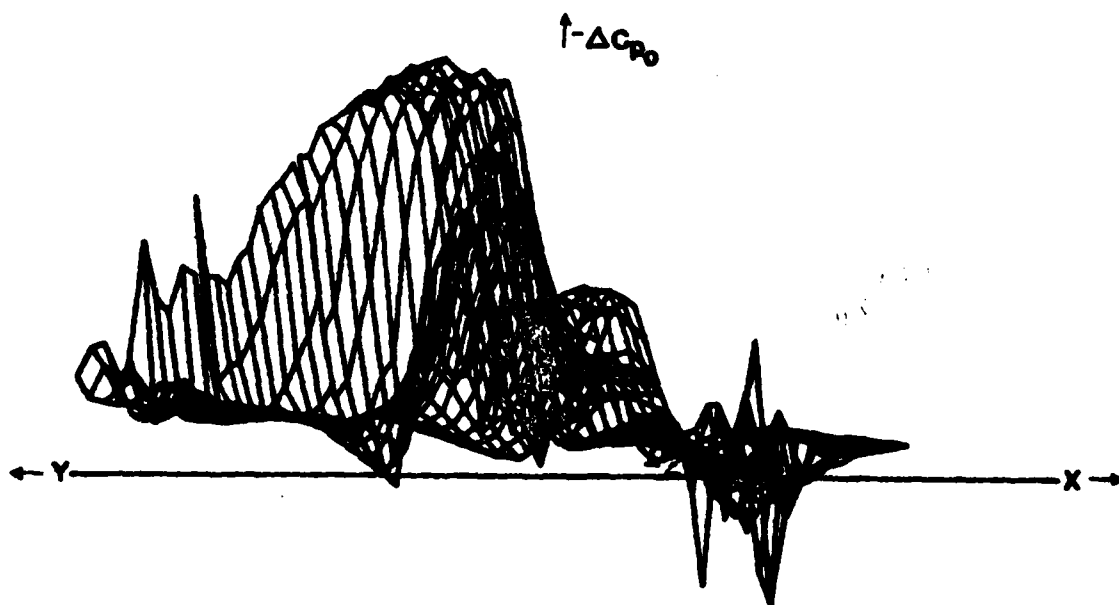Configuration at Streamwise Station 0

79

$\uparrow$ $-\Delta C_{p_0}$

Figure WBC19. ΔC_{p_0} Axonometric Plot for Wing/Body/Canard Configuration at Streamwise Station 0
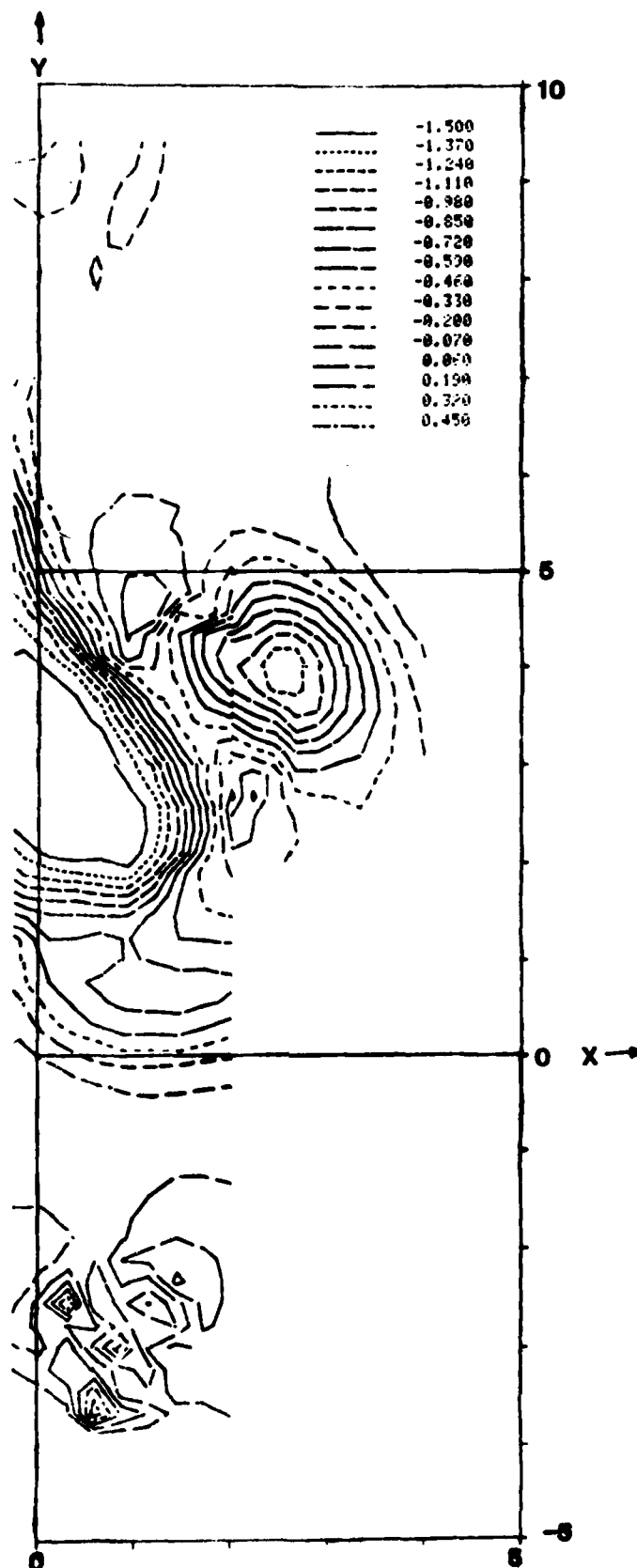
80

Figure WBC20. Contour Plots of ΔC_{Po} in the x-y Plane for Wing/
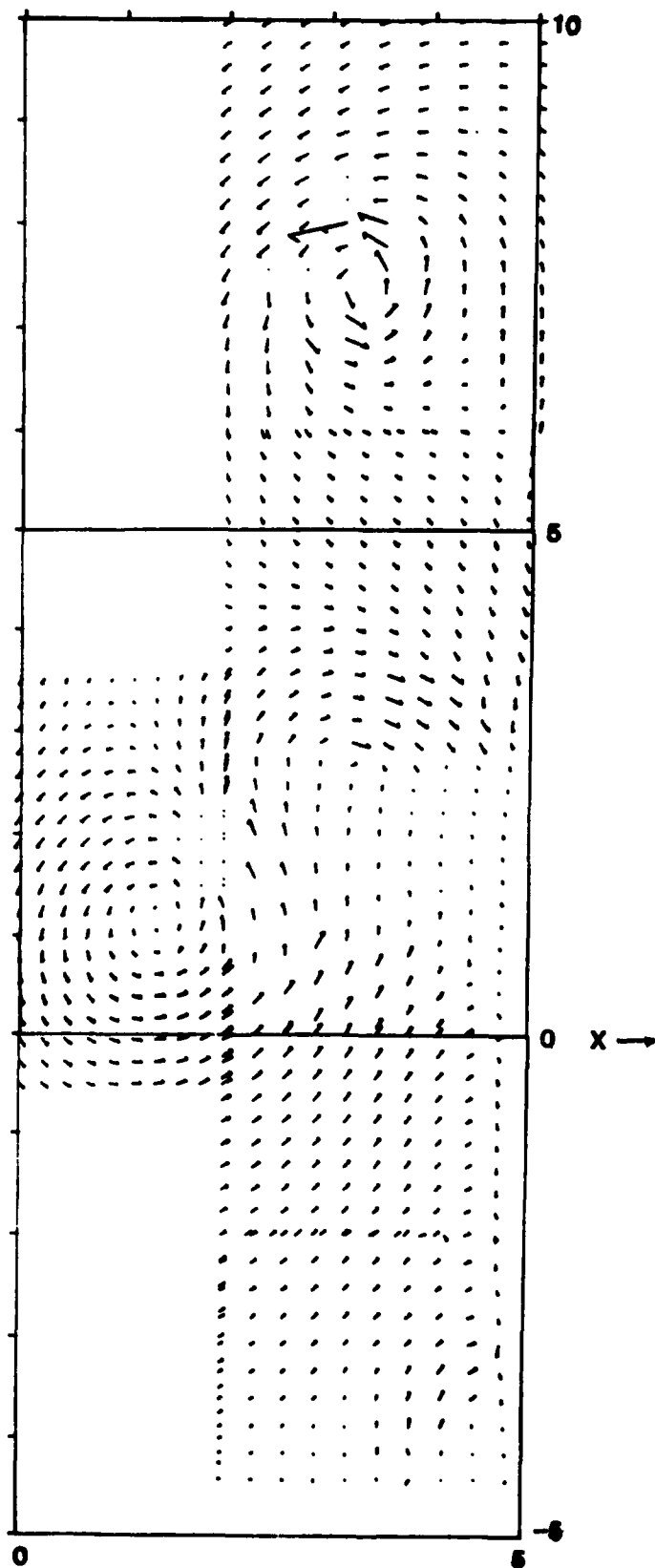Body/Canard at Streamwise Station 0

81

Figure WBC21.   Cross Velocity Vectors in the x-y Plane for Wing/
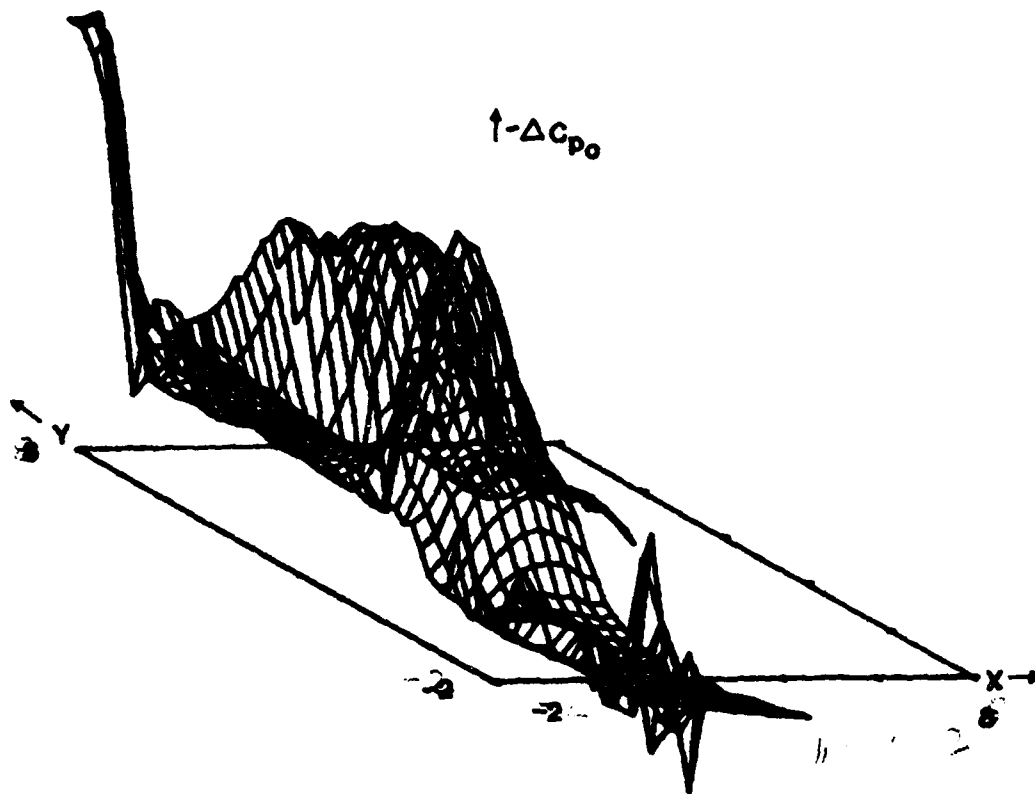Body/Canard at Streamwise Station −2

82

Figure WBC22. ΔC_{Po} Axonometric Plot for Wing/Body/Canard Configuration at Streamwise Station-2

Figure WBC23. ΔC_{Po} Axonometric Plot for Wing/Body/Canard Configuration at Streamwise Station-2

Figure WBC24. ΔC_{Po} Axonometric Plot for Wing/Body/Canard Configuration at Streamwise Station-2

Figure WBC25.   Contour Plots of ΔC_{P_0} in the x-y Plane for Wing/
Body/Canard at Streamwise Station - 2.

86

Figure WBC26.   Cross Velocity Vectors in the x-y Plane for Wing/
Body/Canard at Streamwise Station -4

87

Figure WBC27. ΔC_{p_0} Axonometric Plot for Wing/Body/Canard
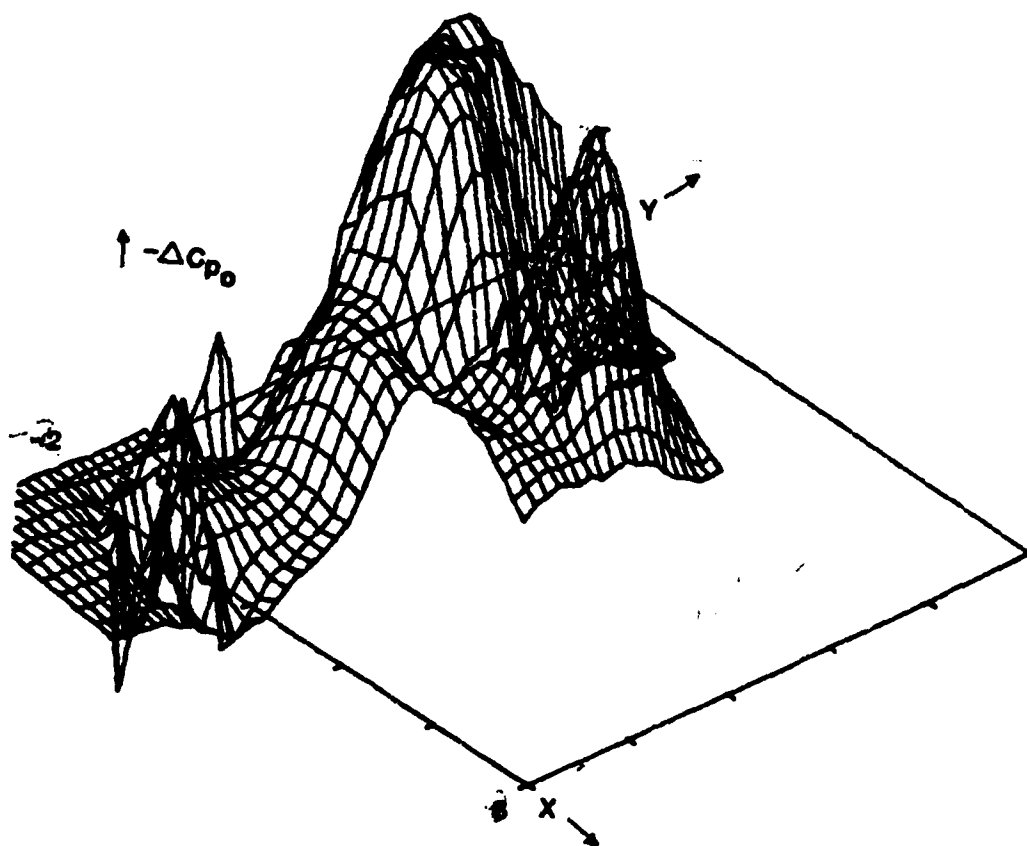Configuration at Streamwise Station-4

88

Figure WBC28. ΔC_{Po} Axonometric Plot for Wing/Body/Canard
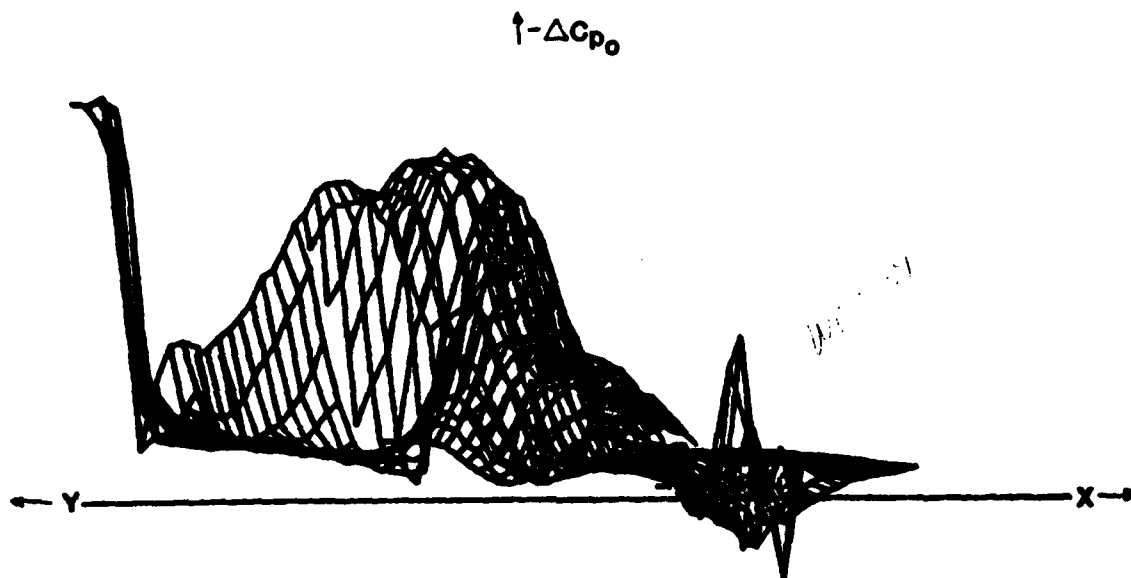Configuration at Streamwise Station-4

Figure WBC29. ΔC_{Po} Axonometric Plot for Wing/Body/Canard
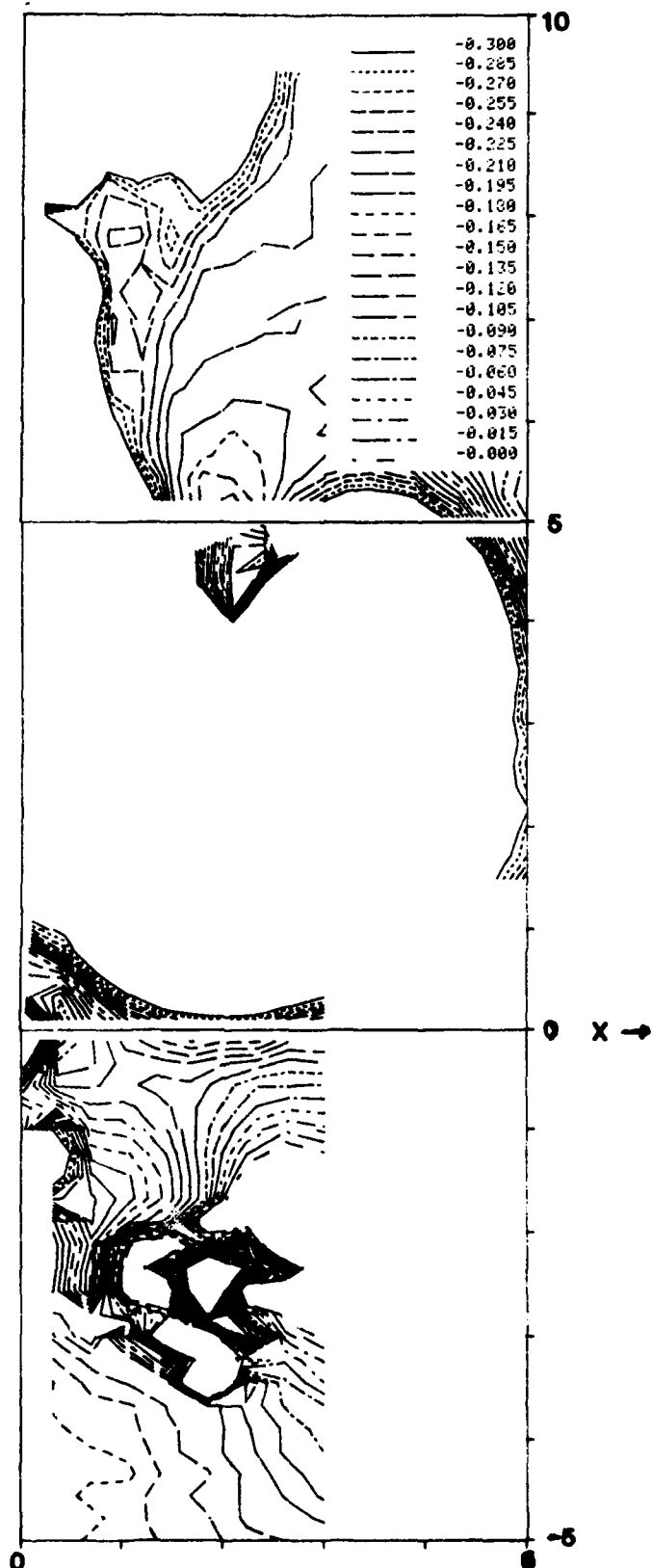Configuration at Streamwise Station-4

89

Figure WBC30. Contour Plots of ΔC_{P_O} in th x-y Plane for Wing/Body/Canard at Streamwise Station-4

90

Figure WBC31.   Cross Velocity Vectors in the x-y Plane for Wing/
Body/Canard at Streamwise Station −6.
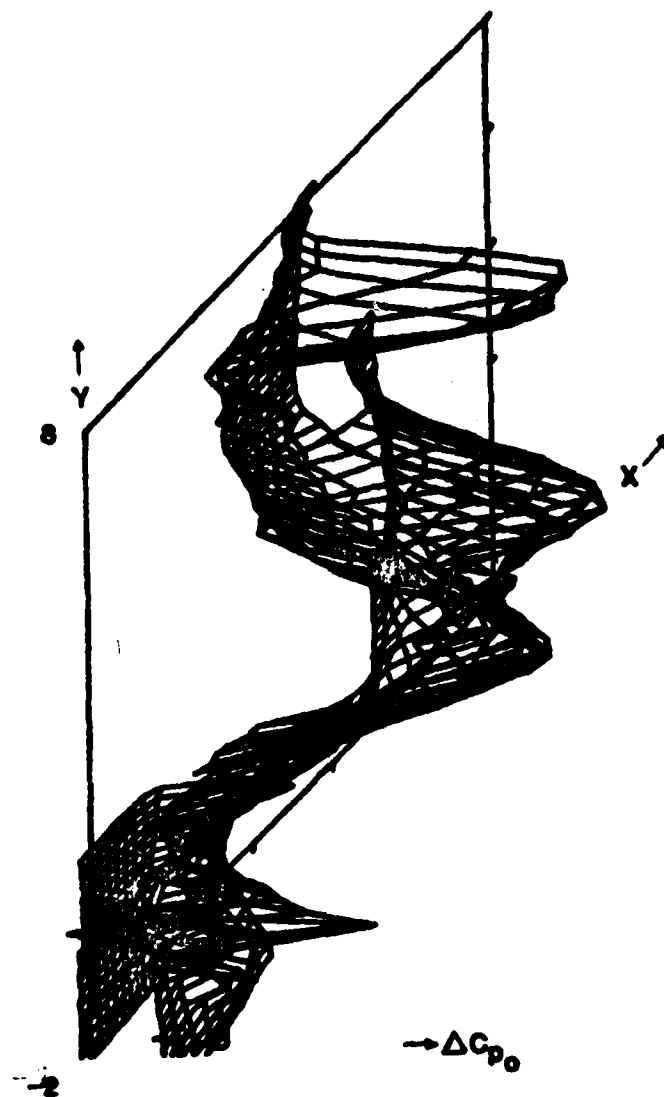
91

$\uparrow -\Delta C_{Po}$

Figure WBC32. ΔC_{Po} Axonometric Plot for Wing/Body/Canard
Configuration at Streamwise Station-6

92

Figure WBC33. ΔC_{Po} Axonometric Plot for Wing/Body/Canard
Configuration at Streamwise Station –6

$\uparrow -\Delta C_{p_O}$

Figure WBC34. ΔC_{p_O} Axonometric Plot for Wing/Body/Canard
Configuration at Streamwise Station-6

94

Figure WBC35.   Contour Plots of ΔC_{Po} in the x-y Plane for Wing/
Body/Canard at Streamwise Station –6

95
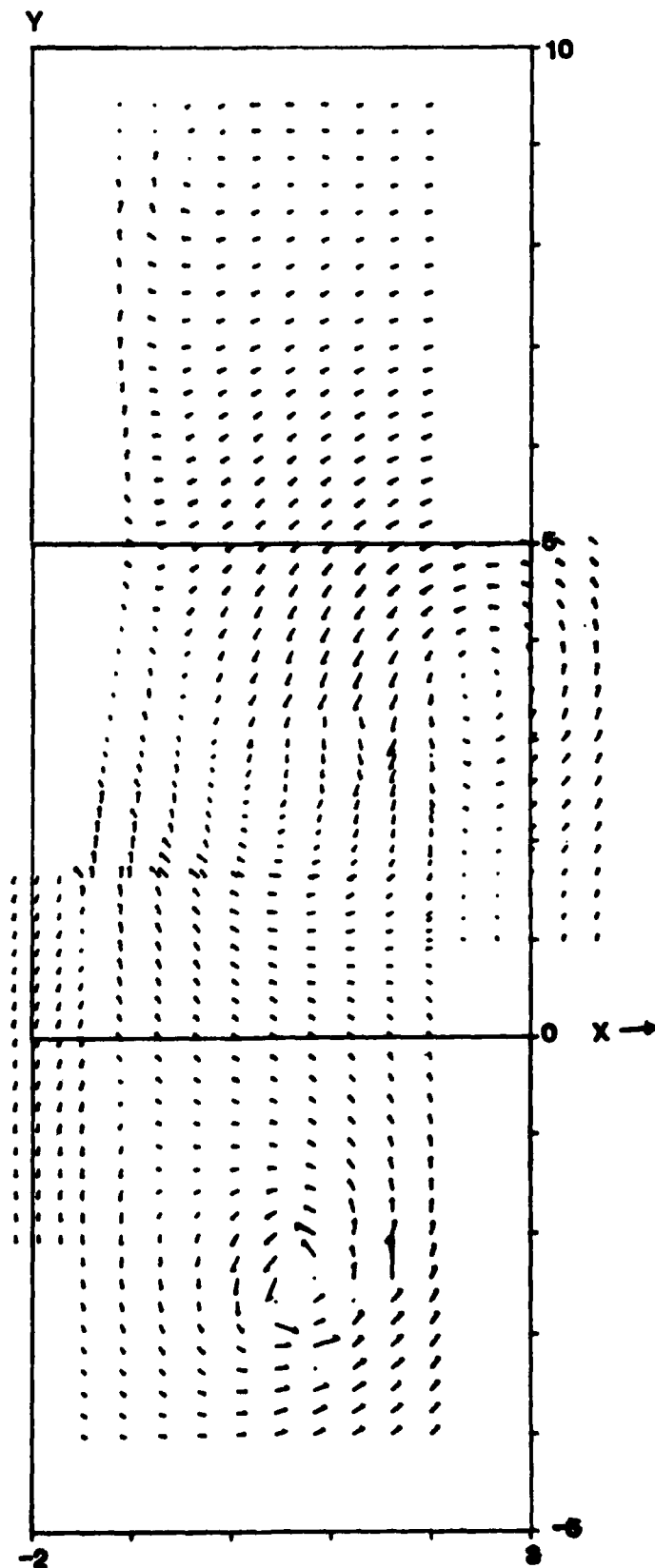
Figure WBC36. Cross Velocity Vectors in the x-y Plane for Wing/
Body/Canard at Streamwise Station – 8

Figure WBC37. ΔC_{p_0} Axonometric Plot for Wing/Body/Canard
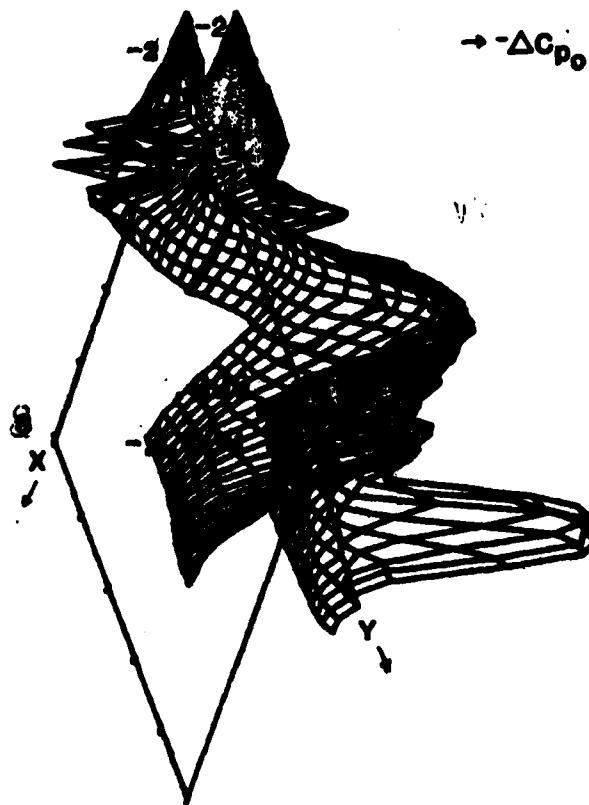Configuration at Streamwise Station-8

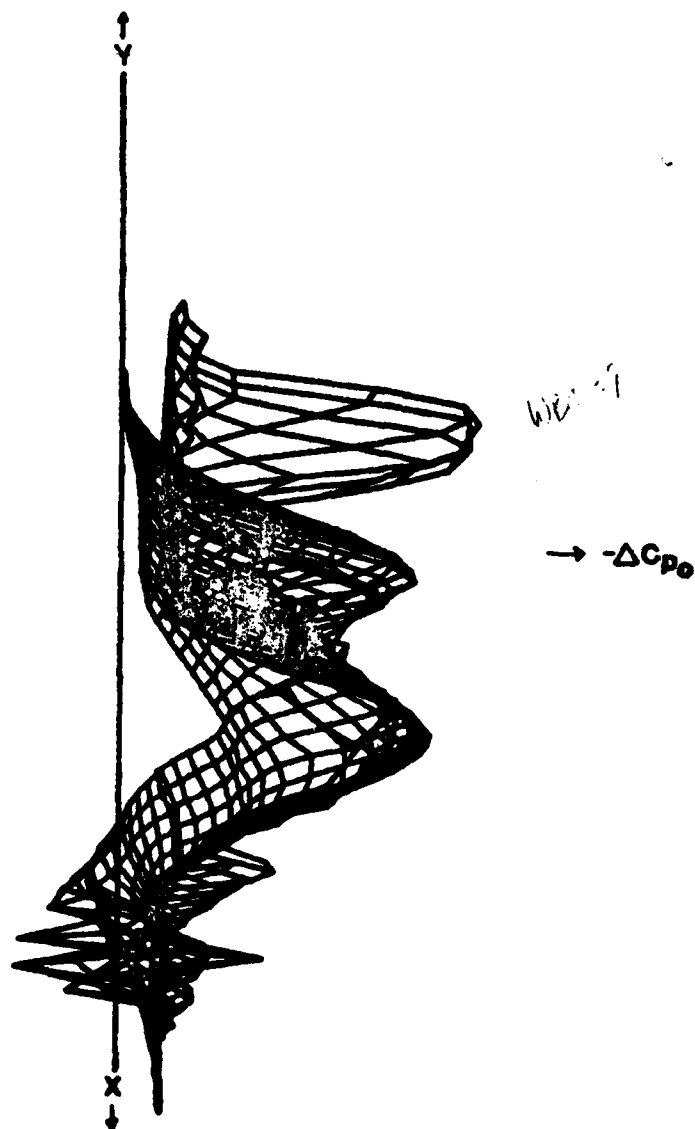Figure WBC38. ΔC_{p_o} Axonometric Plot for Wing/Body/Canard Configuration at Streamwise Station-8

Figure WBC39. ΔC_{Po} Axonometric Plot for Wing/Body/Canard
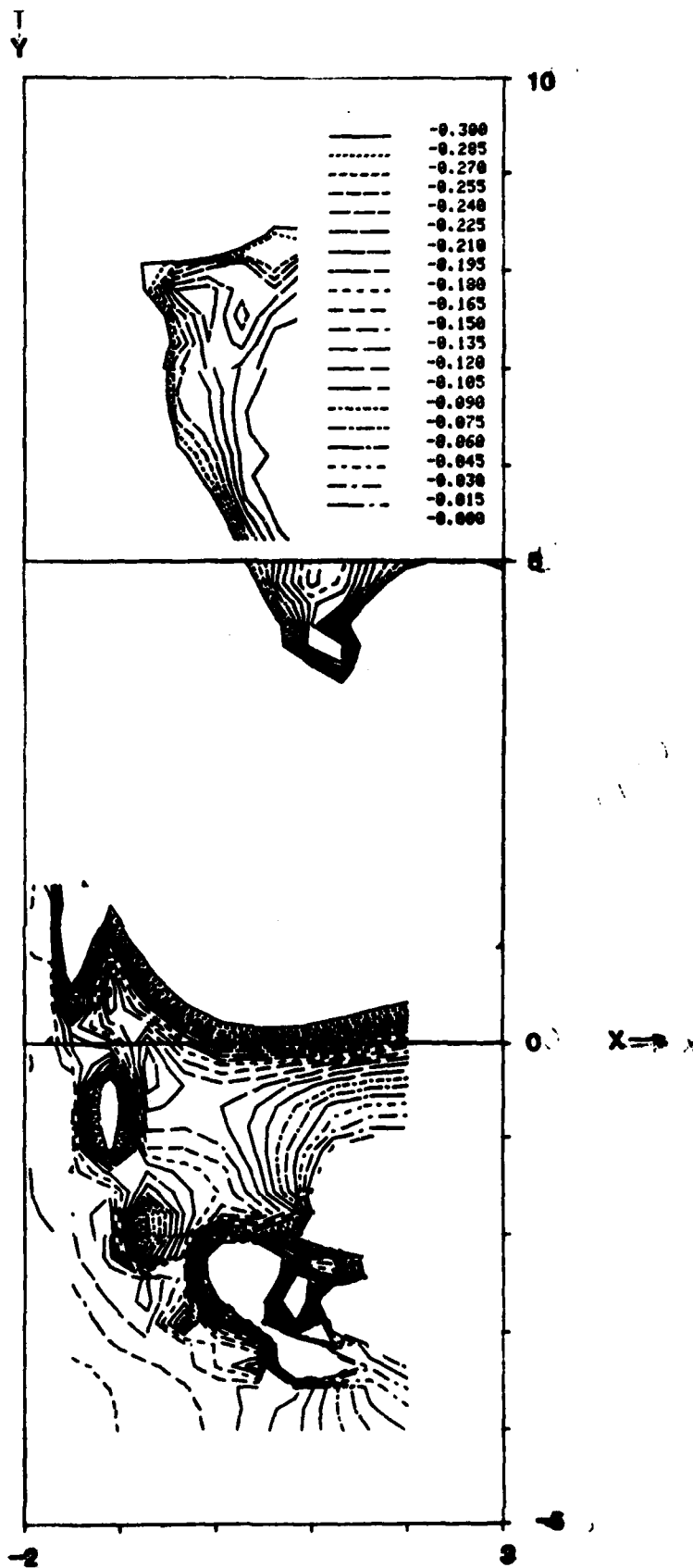Configuration at Streamwise Station-8

Figure WBC40.   Contour Plots of ΔC_{Po} In the x-y Plane for Wing/
Body/Canard at Steamwise Station 8

100

LME
8